

Slow glycinergic transmission mediated by transmitter pooling

Veeramuthu Balakrishnan^{1,2}, Sidney P Kuo^{1,2}, Patrick D Roberts³ & Laurence O Trussell^{1,2}

Most fast-acting neurotransmitters are rapidly cleared from synaptic regions. This feature isolates synaptic sites, rendering the time course of synaptic responses independent of the number of active synapses. We found an exception at glycinergic synapses on granule cells of the rat dorsal cochlear nucleus. Here the duration of inhibitory postsynaptic currents (IPSCs) was dependent on the number of presynaptic axons that were stimulated and on the number of vesicles that were released from each axon. Increasing the stimulus number or frequency, or blocking glycine uptake, slowed synaptic decays, whereas a low-affinity competitive antagonist of glycine receptors (GlyRs) accelerated IPSC decay. These effects could be explained by unique features of GlyRs that are activated by pooling of glycine across synapses. Functionally, increasing the number of IPSPs markedly lengthened the period of spike inhibition following the cessation of presynaptic stimulation. Thus, temporal properties of inhibition can be controlled by activity levels in multiple presynaptic cells or by adjusting release probability at individual synapses.

The duration of postsynaptic currents depends on the kinetics of the neurotransmitter-receptor interaction¹ and the process of exocytosis². Channel gating, affinity and desensitization may determine how single synaptic events participate in neural computations by controlling the duration of receptor activation^{3–7}. Under some conditions, however, the clearance of transmitter appears to be delayed, leading to rebinding of transmitter and a slowing of the synaptic decay, particularly at multi-release site synapses^{8–12}. Developmental changes in synaptic structure or glial apposition can modify the profile of clearance¹³. At mature inhibitory and excitatory synapses, pooling of transmitter sufficient to reactivate postsynaptic receptors appears to be most prominent when transmitter uptake systems are blocked (for example, ref. 14). Thus, it is generally presumed that, under normal conditions, slower synaptic decay rates at inhibitory synapses must reflect either receptor subunit composition¹⁵ or the activity of synapses that are prone to asynchronous release¹⁶. In either case, these mechanisms do not have much power to grade synaptic decays on a fast time scale or over a wide range.

Glycinergic synapses mediate rapid transmission in the brainstem and spinal cord, with typical IPSC decay times of only a few milliseconds¹⁷. GlyRs have multiple binding sites and their occupancy has distinct effects on gating kinetics^{18–20}. Well-timed glycinergic inhibition is important for determining the synaptic output in several brain regions, particularly in the auditory system, where the precise timing of inhibition is critical for information processing²¹. It is generally believed that the decay of glycinergic synaptic currents solely reflects the burst or open duration of GlyR channels^{5,6,20,22}. The relatively incomplete desensitization shown by GlyRs^{5,23} and the slow turnover rates of neurotransmitter transporters^{24,25} suggests the possibility that clearance might determine IPSC decay in some cases. We studied the

determinants of glycinergic IPSC decay in granule cells of the dorsal cochlear nucleus (DCN). The DCN is a laminated structure resembling the cerebellar cortex in which glycinergic and glutamatergic synaptic activity controls the convergence and plasticity of different sensory streams²⁶ (Fig. 1a,b). DCN granule cells receive strong glycinergic input, presumably from Golgi and/or stellate cells²⁷. In contrast with the rapid decay of most glycinergic IPSCs, typically just a few milliseconds in the adult auditory brainstem^{28,29}, glycinergic events last more than tenfold longer in granule cells²⁷. Varying the frequency and intensity of exocytosis and interfering with GlyR interactions using a low-affinity competitive antagonist revealed that transmitter pooling controls the duration of inhibition in an activity-dependent manner.

RESULTS

Correlation between amplitude and decay time of IPSCs

For a given stimulus strength, glycinergic IPSCs varied widely in amplitude, suggesting stochastic fluctuation in the number of vesicles released from trial-to-trial (Fig. 1d). IPSCs, fitted with a double-exponential function, had an average τ_{fast} of 13 ± 2 ms, τ_{slow} of 59 ± 8 ms and %fast of 60 ± 4 ($n = 46$). For each cell, the IPSC decay time was generally longest for the largest events (Fig. 1d,e). Indeed, IPSC amplitude and decay time were positively correlated within cells (mean $r = 0.60 \pm 0.10$, $n = 6$, $P < 0.02$ for 5 out of 6 cells; Fig. 1e). In contrast, the 10–90% rise times of the IPSCs showed no correlation (mean $r = 0.16 \pm 0.08$, $n = 6$, $P > 0.2$ for 6 out of 6 cells; Fig. 1f). The lack of correlation with rise time suggests that larger events are not associated with poorly synchronized release and that extrasynaptic receptors do not contribute to peak current. Rather, these data suggest

¹Oregon Hearing Research Center, ²Vollum Institute and ³Biomedical Engineering, 3181 S.W. Sam Jackson Park Road, Portland, Oregon 97239, USA. Correspondence should be addressed to L.O.T. (trussell@ohsu.edu).

Received 10 November 2008; accepted 19 December 2008; published online 8 February 2009; doi:10.1038/nn.2265

that fluctuation in the amount of transmitter release might lead to variation in the exposure time of receptors to glycine.

The decay time also correlated with the number of axonal inputs activated during the IPSC. Evoked IPSC amplitude increased with stimulus intensity, typically in 2–4 steps, suggesting that each granule cell is contacted by several glycinergic axonal inputs (Fig. 1g). Consistently, this increase in amplitude was linearly correlated with decay time (Fig. 1h,i). Because granule cells are electrically compact, this slowing of the decay could not be a result of escape from voltage clamp^{27,30}. Rather, these observations are consistent with the idea that increasing the number of active synapses leads to transmitter pooling.

Pooling of transmitter release following repetitive exocytosis

To determine whether such pooling of transmitter could be enhanced by repetitive synaptic stimuli, we activated synapses by varying the number (1–10 at 100 Hz) or frequency (20–200 Hz) of stimuli. The decay time positively correlated with the number of stimuli ($r = 0.9$, $P < 0.0001$, slope = 4.8 ms per added stimulus; Fig. 1j,k). Increasing stimuli from 1 to 10 increased the decay by $176 \pm 27\%$ ($n = 5$,

$P = 0.0029$). Elevating the stimulus frequency tenfold, from 20 to 200 Hz, increased the decay time by $158 \pm 44\%$ ($n = 7$, $P = 0.012$; Fig. 1l,m). To test whether the increased decay time following trains could be a result of modulatory effects of GABA or glutamate released from other nerve fibers, which might cause a Ca^{2+} rise in the postsynaptic cell, we repeated single and 100-Hz train stimuli in the presence of $20 \mu\text{M}$ (*RS*)- α -ethyl-4-carboxyphenylglycine (E4CPG) and (*RS*)- α -cyclopropyl-4-phosphonophenyl-glycine (CPPG) to block group I–III mGluRs and $10 \mu\text{M}$ CGP-55845 to block GABA_B receptors. In seven experiments, train stimulation increased the decay time by $115 \pm 22\%$, indicating that slower decays are not produced by activation of such modulatory pathways (data not shown). Finally, we tested whether the slow glycine IPSC could reflect an artifact of the high intracellular Cl^- used in the voltage clamp experiments³¹ and found that slow decays remained when Cl^- was reduced to 10 mM (single IPSC decay, 17.4 ± 4.1 ms; IPSC decay after train, 56.6 ± 11.9 ms; $n = 5$).

The increased decay time following train-evoked IPSCs might result from enhancement of delayed quantal releases, as has been shown at

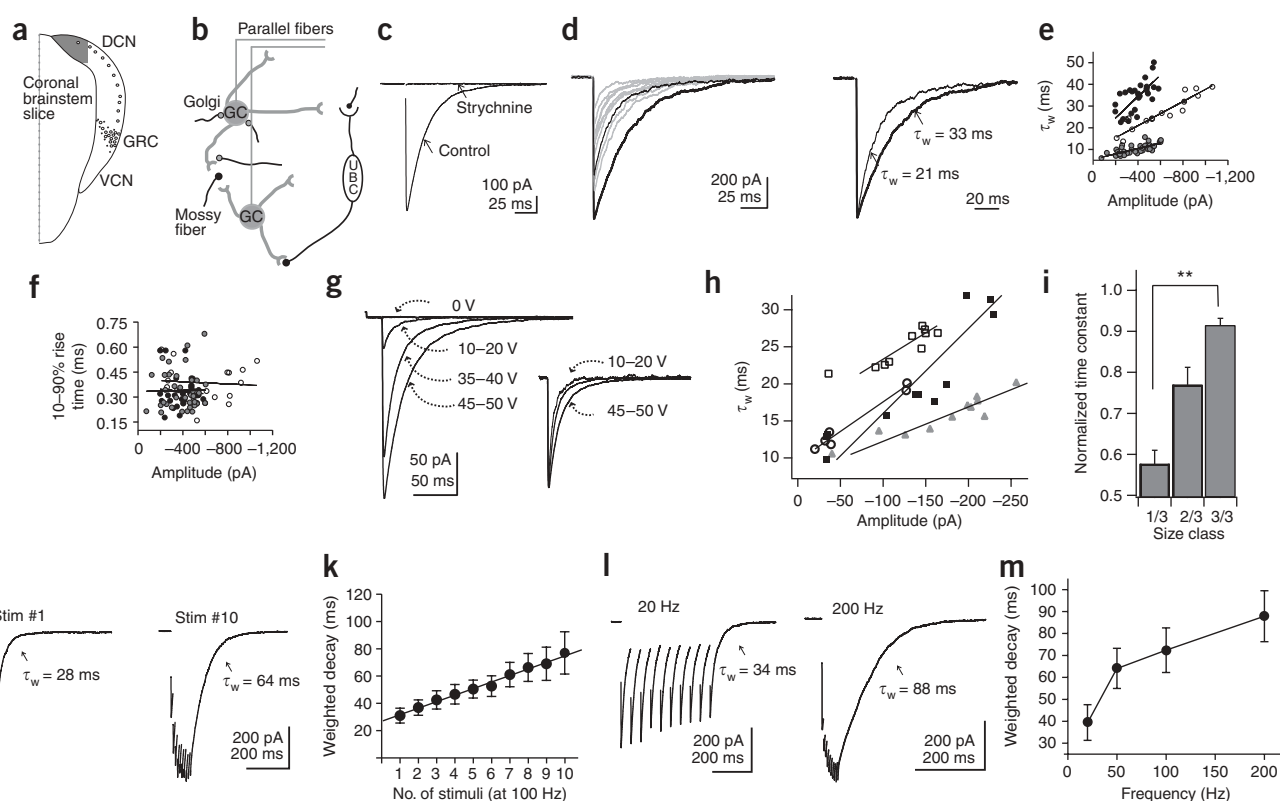


Figure 1 Granule cells in the DCN and their glycinergic postsynaptic currents. (a) Schematic representation of the cochlear nucleus in a coronal brainstem slice, showing the distribution of granule cells (circles) in the DCN and the granule cell region (GRC). VCN, ventral cochlear nucleus. (b) Synaptic inputs to granule cells. Granule cells (GCs) receive excitatory inputs through mossy fibers and the unipolar brush cells (UBC). Inhibitory inputs are assumed to be from the Golgi/stellate neurons. (c) Averaged glycinergic IPSC from a granule cell under control conditions and after $0.5 \mu\text{M}$ strychnine application. (d) Example traces of glycinergic IPSCs on synaptic stimulation. Two sample IPSCs of different sizes are shown in thick and thin black lines. On the right, these IPSCs were normalized and their corresponding weighted decay times are shown. (e) The weighted decay constants of the IPSCs positively correlated with the amplitude. Plot shows the values from three cells and their corresponding regression line. The linear fits in the three plots have $r = 0.92$, 0.68 and 0.76 with $P < 0.0001$ for all. (f) IPSC rise times and amplitudes had no correlation. The values from three cells, plotted as rise time and amplitude. Linear fits are insignificant for all cells ($P > 0.05$). (g) Example IPSCs evoked at various voltages. The inset shows the traces normalized, revealing that responses to smaller stimuli decayed more quickly. (h) Correlation of amplitude and weighted decay as stimulus strength was changed in four neurons. Correlation coefficients were 0.88 , 0.91 , 0.93 and 0.99 ($P < 0.002$). (i) The normalized amplitudes of the responses were grouped into upper (1/3), middle (2/3) and lower (3/3) thirds of the population and their corresponding decay times averaged (9 cells, 15–36 measurements per category, $P < 0.002$ between categories). (j) Examples of glycinergic IPSCs evoked with one and ten stimuli (10-ms interval). (k) Weighted decay times of the IPSCs against number of stimuli (100 Hz) from five cells. (l) Ten IPSCs delivered at 20 and 200 Hz. (m) Weighted decay times from seven cells at different frequencies. Comparison of decay times at different frequencies (20–50 Hz, $P < 0.01$; 50–100 Hz, $P < 0.05$; 100–200 Hz, $P < 0.001$). Error bars represent \pm s.e.m.

some GABAergic synapses¹⁶. However, such delayed releases were not as prominent as in GABAergic synapses, and so were probably not of sufficient frequency to slow the current decay. To determine whether asynchronous release could have been detected, we substituted 8 mM Sr²⁺ for extracellular Ca²⁺ and delivered synaptic stimuli at low or high frequency. With Sr²⁺, asynchronous quantal releases were clearly observed after single or multiple stimuli (Fig. 2a,b) and showed a marked increase in frequency over the sparse delayed events seen in control solution. Delayed quantal release events were sampled, aligned and averaged to assess their amplitude and duration. The decay of quantal events was compared with that of single and train-evoked responses in normal Ca²⁺ solutions in the same cells, indicating that quantal currents decayed nearly twice as fast as the response to single presynaptic stimuli (Fig. 2c,d). Given the mean size of these events (33.5 ± 16.5 pA, *n* = 5 cells; Fig. 2c), they would have been visible during the decay of evoked currents in Ca²⁺-containing solutions if they were responsible for slowing the decay by several fold. However, in six cells in the absence of Sr²⁺, we detected by eye an average of only 0.17 ± 0.06 quantal events per trace during a 500-ms window after the train (data not shown, 506 traces total). This was determined after ‘linearizing’ the current decay after a train by subtracting a fitted bi-exponential curve from each trace. Although some slowing of the evoked response is expected because of the profile of exocytosis, such asynchrony is probably not great, as the rise time of quantal and evoked events were not significantly different (*P* > 0.05) (Fig. 2d).

We tested this further by using the average amplitude and decay of quantal responses recorded in Sr²⁺ to deconvolve the release time course expected if the slow IPSC decay was solely the result of release rate and channel kinetics (Fig. 2e,f). We examined the release rate after the tenth stimulus in a train, when the current had decayed by 63%, a point at which quantal releases should have been easily apparent from the baseline. This analysis predicted an average release rate at that time of 0.18 ± 0.02 per ms, or roughly one event every 5.6 ms (mean from three neurons, with three measurements per cell), which was much higher than the measured rate of 0.17 releases per 500 ms. It may be argued that many releases were undetected because of a high signal-to-noise ratio. However, the noise level was quite low and in some cells it was possible to easily resolve single GlyR channel currents underlying the IPSCs (Fig. 2g,h), as shown previously²⁷. Thus, in a single stimulus or with repeated stimuli, the slower IPSC decay is the result of a more gradual transmitter clearance rather than a gradually decaying rate of release.

Release probability influences the decay time

If enhanced synaptic activity leads to slowing of transmitter removal and, consequently, of the synaptic decay time, then release probability and decay time should also correlate. To test this idea, we compared the IPSCs evoked in different extracellular Ca²⁺ concentrations. Raising the release probability by increasing the Ca²⁺ concentration between 1 and 4 mM increased the mean synaptic decay time (Fig. 3a,b). Halving bath Ca²⁺ from 2 to 1 mM reduced the decay time by 26 ± 3% and the

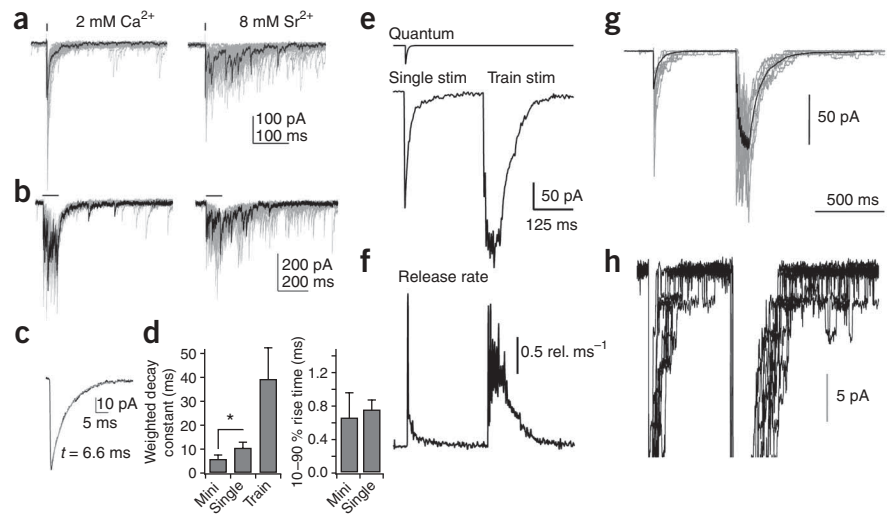


Figure 2 Asynchronous release. (a) Evoked responses in 2 mM Ca²⁺ and 8 mM Sr²⁺. (b) Response to ten stimuli (100 Hz) in 2 mM Ca²⁺ and 8 mM Sr²⁺. In all cases, asynchronous release events are clearly visible. Black trace highlights one of 25–51 traces in each panel. All data shown are from one cell. (c) Averaged delayed release IPSC from data shown in a and b. (d) Decay time constant for delayed release events (mini), and response to single stimuli or trains of ten shocks at 100 Hz. Rise time of quanta and evoked responses were not significantly different (*P* > 0.05). * indicates *P* < 0.01 (*n* = 5 cells). (e) Simulated quantal current $-34 \text{ pA} \times (1 - e^{-t/\tau_{\text{mini}}})^2 (e^{-t/\tau_{\text{mini}}})$ and an unaveraged trace showing responses to a single stimulus and to a train of ten stimuli delivered at 100 Hz. (f) Deconvolved release rate from traces in e. (g) Ten low-noise traces from one cell showing response to a single stimulus and a train of ten stimuli. The average of 64 such traces is superimposed in black (decay times were 38 ms and 89 ms for single and train responses). (h) Same sweeps as g, shown at higher gain to illustrate single-channel currents. Error bars represent ± s.e.m.

amplitude by 52 ± 5% (*P* < 0.001 for both, *n* = 6). Doubling Ca²⁺ nearly doubled both the decay time and amplitude (80 ± 16% and 87 ± 19% increases, respectively; *P* < 0.01, *n* = 5). Notably, the extent of changes in amplitude and decay time induced by changes in Ca²⁺ resembled those seen with changes in stimulus strength (Fig. 1h,i). This relationship implies that release sites from different axons are so close that increasing the number of activated axons or the probability of release from each axon has an equivalent effect on the decay time. The relation between amplitude and decay time also predicted the mean values that we obtained for quantal currents recorded in Sr²⁺ solutions (Fig. 2b).

Glycine transporters shape the IPSC

Transmitter spillover between synapses is often enhanced after blockade of transmitter transporters^{3,14,32,33}. Given the dominant role of slow glycine clearance shaping IPSCs in granule cells, we asked whether uptake systems are involved in regulating the decay of glycinergic events. On bath application of ALX-5407 (20 μM), a blocker of glial glycine transporter (GlyT1)³⁴, the decay time of glycinergic IPSCs on single stimulation increased by 43 ± 10% (19.1 ± 3.1 to 26.5 ± 4.4 ms, *n* = 8, *P* = 0.019, paired *t* test; Supplementary Fig. 1 online). In contrast, no significant change in the amplitude was apparent (29 ± 19% change, *n* = 8, *P* = 0.145). ALX-5407 also increased the decay following trains of ten stimuli at 100 Hz by 36 ± 9% (44 ± 5 to 60 ± 8 ms, *n* = 7, *P* = 0.009, paired *t* test). A second series of experiments were carried out with 20 μM ORG-25543, an antagonist of the neuronal glycine transporter GlyT2 (ref. 35). As with the GlyT1 antagonist, the decay time after single or 100-Hz train stimuli was lengthened following blockade of neuronal glycine uptake (singles: from 17.5 ± 2.1 to 23.7 ± 2.6 ms, 43 ± 20% increase, *n* = 8, *P* = 0.03, paired *t* test; trains: from 52.9 ± 7.5 to 73.6 ± 12.1 ms, 40 ± 12%, *n* = 5,

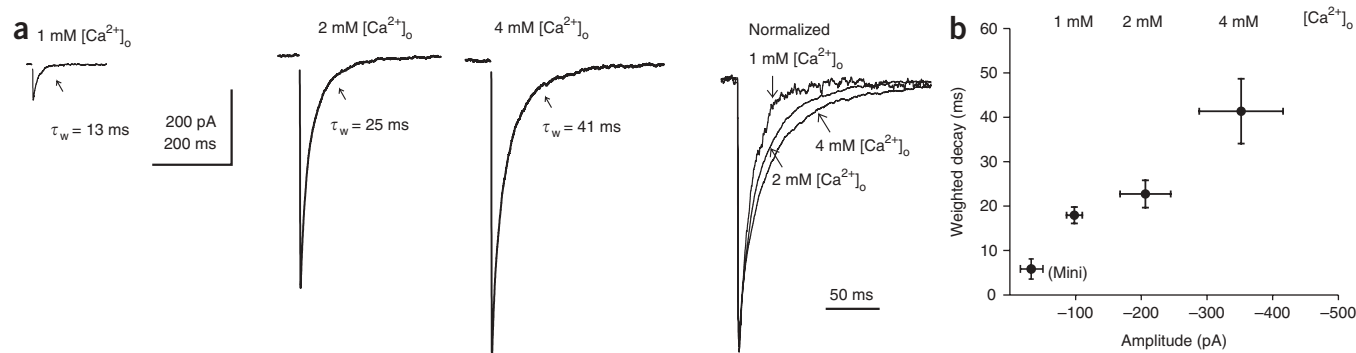


Figure 3 Increasing release probability slows IPSC decay time. **(a)** Averaged glycinergic IPSCs recorded in different bath Ca^{2+} concentrations. Corresponding weighted decay constants are also shown. **(b)** Relationship between amplitude and decay time in three Ca^{2+} concentrations, as indicated ($n = 5$ cells). Lower left, mean amplitude and decay time for delayed release events (mini) for 5 cells. Error bars represent \pm s.e.m.

$P = 0.04$, paired t test) with no change in amplitude ($P = 0.66$) (Supplementary Fig. 1). Thus, glial and neuronal glycine transporters have a role in shaping synaptic responses, but do not prevent transmitter rebinding and reactivating receptors after single synaptic stimuli.

Multivesicular release determines peak IPSC amplitude

The effect of increasing stimulus strength on IPSC decay is probably the result of the pooling of transmitter from neighboring release sites. However, the slowing of IPSC decays after increase in release probability could be explained by either pooling or multivesicular release, in which multiple vesicles are released from individual release sites; either situation could, in principle, lengthen the time for transmitter to fall below the level needed to activate receptors. SR-95531 (gabazine), a well-known GABA_A receptor antagonist, has been shown to act as a low-affinity competitive antagonist of native or heterologously expressed GlyRs^{20,36,37}. We used SR-95531 to test for multivesicular release and to probe transmitter lifetime in the cleft. The mean amplitude of IPSCs in 2 mM bath Ca^{2+} decreased by $71 \pm 2\%$ ($n = 10$, $P = 0.0005$) in the presence of 300 μ M SR-95531 (Fig. 4a,b). The effectiveness of the antagonist was then tested in 1 or 4 mM Ca^{2+} , revealing that block by SR-95531 increased when quantal release was reduced (Fig. 4b). These data indicate that multiple vesicles must be released at individual release sites in response to single stimuli in 2 mM bath Ca^{2+} .

Having established the presence of multivesicular release, we next examined the degree of inhibition by SR-95531 in 2 mM bath Ca^{2+} in

the presence of ALX-5407 (20 μ M) and ORG-25543 (20 μ M). This approach explored the view that the apparent competition between the transmitter and antagonist on the peak current is influenced by spillover of transmitter between synaptic sites. In the presence of both blockers, however, the percent inhibition was $68 \pm 6\%$ ($n = 4$), which was not different from the control value of 71% (data not shown). We sought to determine the degree of inhibition produced by 300 or 150 μ M SR-95531 (five cells each) on delayed release events recorded in 8 mM Sr^{2+} following train stimuli, but found that the antagonist reduced the detection rate of these events too severely. In those experiments, the amplitudes of low-frequency evoked IPSCs were reduced by $88 \pm 3\%$ and $77 \pm 4\%$ by 300 μ M and 150 μ M SR-95531, respectively, and it is therefore not surprising that most quantal events would be undetectable. Given that the degree of block was lowest for evoked responses in the presence of Ca^{2+} , we conclude that multivesicular release must determine the peak amplitude of evoked IPSCs.

To further explore the ability of the SR-95531 to interact with receptors on the time scale of transmitter release and clearance, we examined the response to stimulus trains. During trains, the IPSC amplitude (foot to peak) of later events grew smaller, presumably as a result of synaptic depression and/or receptor saturation. If the GlyRs are progressively saturated by accumulating transmitter, the relative magnitude of this decline in amplitude should be reduced by SR-95531. We normalized the first IPSCs in trains recorded in controls and SR-95531-treated neurons so that the relative amplitude of the later IPSCs in the train could be compared with the first IPSC. The ratio of

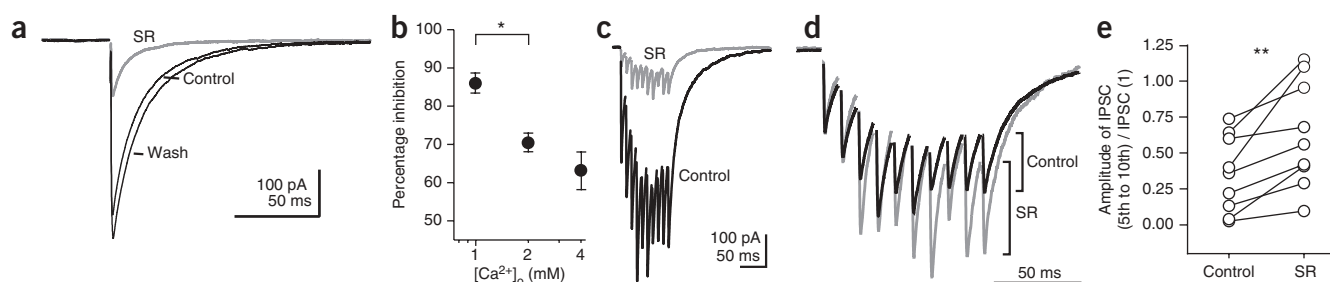


Figure 4 Probing multivesicular release and receptor saturation using a weak antagonist of GlyRs, SR-95531. **(a)** Block of IPSCs by 300 μ M SR-95531 (SR). **(b)** Percent reduction in IPSC amplitude by 300 μ M SR-95531 in different Ca^{2+} concentrations (4–9 cells per point). Values for 1 and 2 mM Ca^{2+} were significantly different ($P < 0.05$). **(c)** SR-95531 inhibition of responses to a train of ten IPSCs at 100 Hz. **(d)** Traces in **c** were normalized to the first IPSC in the train. Amplitudes of later IPSCs in the train were measured from the foot to peak, as indicated. **(e)** Summary of the peak amplitudes of the last five IPSCs in a train in control and in the presence of SR-95531 for ten experiments in which the amplitudes were normalized to first IPSC. A comparison of the responses in control and SR-95531 revealed that there was a significant increase in the relative amplitude of later IPSCs ($P < 0.0015$, paired t test) indicating that SR-95531 relieves saturation during high-frequency trains. Error bars represent \pm s.e.m.

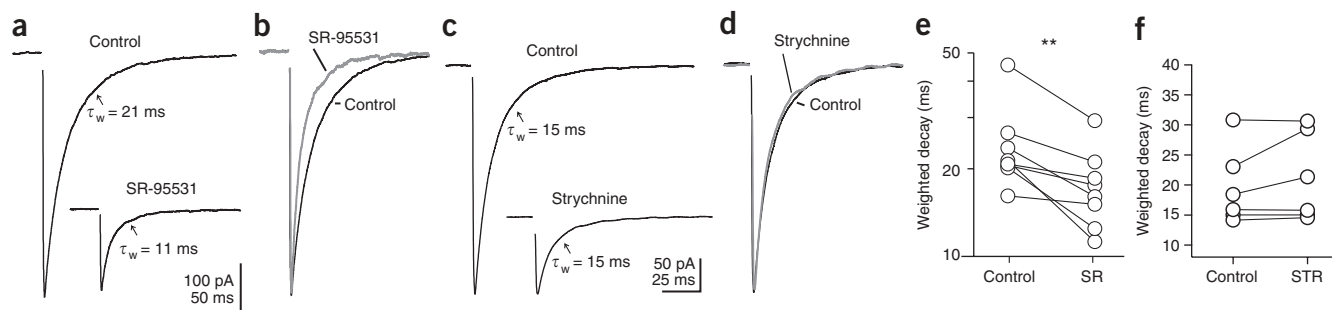


Figure 5 SR-95531 accelerates the decay of IPSCs. **(a)** Example of averaged and **(b)** normalized glycinergic IPSCs on single stimulation in control and in the presence of 300 μM SR-95531. **(c,d)** Example of averaged **(c)** and normalized **(d)** traces with and without 200 nM strychnine. **(e,f)** Effect of SR-95531 (SR) and strychnine (STR) on weighted decay time. Paired *t* tests were significant only for the SR-95531 trials ($P < 0.003$).

the mean of the last five events to the first IPSC (IPSC₅₋₁₀/IPSC₁) in controls was significantly less than in SR-95531-treated neurons (paired *t* test, $P = 0.0015$, $n = 10$; **Fig. 4c–e**), indicating that receptor saturation increases during high-frequency IPSCs.

If the concentration of glycine falls gradually, then the low-affinity antagonist should become progressively more effective at preventing rebinding of glycine to its receptor. A consequence of this effect would be an acceleration of the decay of synaptic current. Supporting this hypothesis, the decay of IPSCs during single and train stimulation was accelerated by SR-95531 (**Fig. 5**). On application of SR-95531 during single stimulation, the mean weighted decay time decreased significantly from 23 ± 3 to 17 ± 2 ms (25 \pm 5% decrease, $n = 9$, $P = 0.003$, paired *t* test; **Fig. 5a,b,e**). During train stimulation, the weighted decay time decreased significantly from 58 ± 8 to 47 ± 7 ms (21 \pm 3% decrease, $n = 10$, $P = 0.0001$, paired *t* test). As a control, we examined the effect of a submaximal concentration of strychnine, a high-affinity antagonist. Strychnine (200 nM) had no effect on the synaptic decay time, despite blocking the IPSC to a nearly identical level (**Fig. 5c,d,f**). Thus, we conclude that multivesicular release of glycine leads to a delay in the clearance of transmitter from the synaptic cleft and a prolonged IPSC decay.

Predictions of kinetic modeling

Our data suggest that the lifetime of transmitter in the synaptic cleft can change with stimulus condition and can therefore regulate the decay time of IPSCs. To explore what transmitter time courses are consistent with these results, we modeled the kinetics of GlyR gating using different glycine concentration transients. We adopted a previously described

model¹⁸ that is based on cell-attached single-channel recordings and modified it to include desensitization and competitive antagonism (see **Supplementary Results** and **Fig. 2** online for a complete description of the model and its results). This model, and results from previous studies, highlights features that suggest a unique ability of the GlyR to respond to changes in transmitter transients with changes in synaptic decay time^{5,19,38–41}, most notably the presence of multiple binding sites and associated open states with distinct burst times and comparatively little desensitization. Transmitter transients at single synaptic sites are typically quite rapid. Although peak levels of transmitter reach the millimolar range, diffusion models predict that the majority of transmitter is cleared rapidly and can be approximated with a major exponential component of less than 100 μs and a slower component of a few ms⁴². We explored the behavior of the model with a peak of 6 mM and a fast decay of 80 μs , followed by a slower component with a peak of 15 μM and a 5-ms decay time (see **Supplementary Results** and **Figs. 3–6** online for more extensive testing of parameters). This resulted in an IPSC with an 8.3-ms exponential decay time (**Fig. 6a**), similar to the decay of asynchronous quantal currents (**Fig. 2c,d**), but faster than typical evoked events (**Fig. 2b**). Indeed,

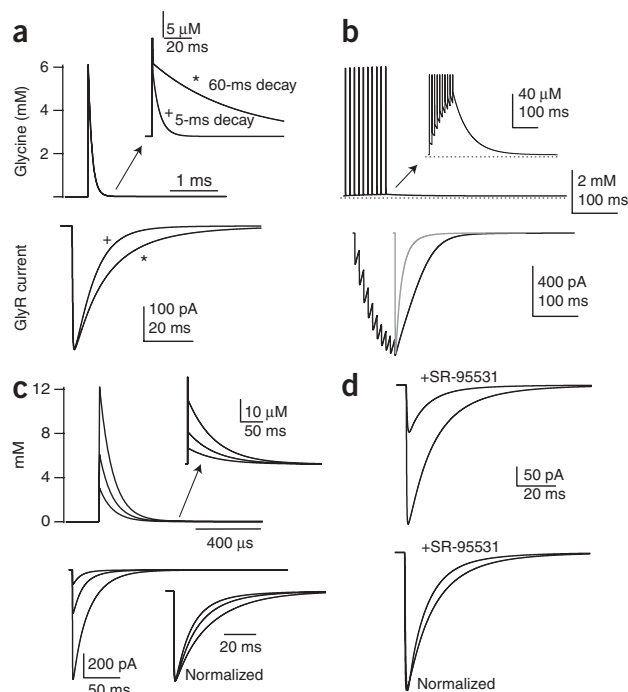


Figure 6 Simulation of IPSCs. **(a)** The glycine transient had a peak of 6 mM and a fast decay constant of 80 μs . Inset, the same traces are shown but with a different scale to illustrate the two slow decay constants, 5 and 60 ms, used in the simulation. These transients were then used to drive a previously described GlyR model¹⁸ (see **Supplementary Results** for details) and the resulting traces are shown below. The weighted decay times of these were 8.3 and 16.6 ms. **(b)** The transient with the 60-ms slow decay constant was used to create the response to ten stimuli at 100 Hz, resulting in a large buildup of transmitter. The resulting IPSC decayed with a 49.9-ms decay constant. The gray trace is the scaled response to the single stimulus shown in **a**. **(c)** The glycine transient in **a** was scaled by 0.5 or 2 to simulate an increase or decrease in multivesicular release. Such changes altered peak synaptic responses (indicating that receptors were not saturated by one vesicle) and changed synaptic current decay time. **(d)** Simulation of IPSCs with the 60-ms slow decay constant and the effects of 300 μM SR-95531. The antagonist both inhibited the IPSC and accelerated its decay (see **Supplementary Results** for implementation of antagonist model and further simulations).

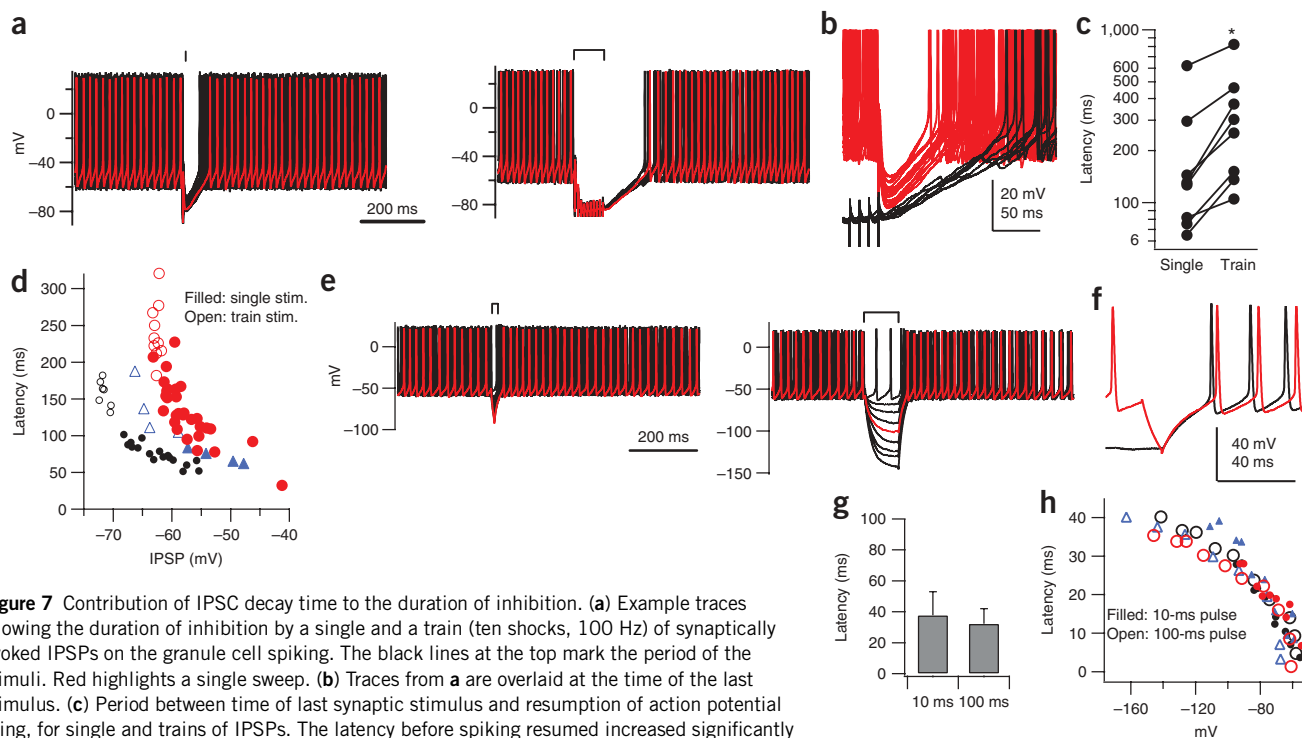


Figure 7 Contribution of IPSC decay time to the duration of inhibition. **(a)** Example traces showing the duration of inhibition by a single and a train (ten shocks, 100 Hz) of synaptically evoked IPSPs on the granule cell spiking. The black lines at the top mark the period of the stimuli. Red highlights a single sweep. **(b)** Traces from **a** are overlaid at the time of the last stimulus. **(c)** Period between time of last synaptic stimulus and resumption of action potential firing, for single and trains of IPSPs. The latency before spiking resumed increased significantly following a train of IPSPs ($n = 8$, $P < 0.0015$). **(d)** Relationship between peak of IPSP and latency to spike firing for three cells. Latency increased sharply with larger IPSPs, consistent with longer lasting synaptic conductance. **(e)** Example traces in which firing was interrupted by negative current steps (marked by brackets) of different amplitude (range of -5 to -50 pA) for 10 ms (left sweeps) or 100 ms (right sweeps). **(f)** Example of overlaid responses at termination of 10- and 100-ms current pulses that hyperpolarized the neuron to a potential near -80 mV. **(g)** Latency to spike firing after 10- and 100-ms pulses for IPSPs reaching near -80 mV (-75 mV to -82 mV). **(h)** Relationship between the most negative point of hyperpolarization and the resulting latency to firing for six cells. These data show a sublinear relation between voltage and latency, suggesting a maximal repriming of A-type K^+ current. Error bars represent \pm s.e.m.

substantial slowing of the IPSC decay (without concomitant slowing of the rise time) could only be obtained by markedly lengthening the duration of the smaller, second component of decay. This immediately implies that rebinding of glycine to the receptor must occur during the IPSC decay. Moreover, given that very slow decay components such as these are inconsistent with diffusion from a single synaptic site⁴², the slow decay must reflect transmitter pooling from many synaptic sites.

IPSC decays as slow as those observed experimentally for single stimuli in 2 mM Ca^{2+} required a slow component of at least 60 ms (Fig. 6a and Supplementary Fig. 3). During train stimuli, this slow component summated and predicted a marked slowing of the simulated IPSC to a similar extent as that seen experimentally (Fig. 6b); such slowing of train responses was not seen when the 60-ms glycine decay was reduced back to 5 ms (Supplementary Fig. 4). The IPSC decay could also be markedly affected by scaling the amplitude of the glycine waveform 0.5–2-fold to mimic the effects of multivesicular release (Fig. 6c); however, this effect required the additional presence of pooling (see Supplementary Fig. 6). Finally, we mimicked the effect of the weak antagonist SR-95531, using the parameters of a previously described model³⁶ (see Supplementary Results). At 300 μ M SR-95531, the model predicted (Fig. 6d) that the IPSC would be reduced to 34% of control (compared with 30% seen experimentally) and that the weighted decay time after single shocks or 100-Hz trains would be reduced by 28% and 29% (compared with 27% and 28% seen experimentally). The magnitude of the effect of the antagonist on decay time could only be reproduced if a very slow phase of clearance was assumed (Supplementary Figs. 5 and 6). When the antagonist

simulation was retested using a transient with cleft glycine concentration scaled down by half (simulating reduced multivesicular release, as in Fig. 6c) the peak response was reduced to 11% of control, as compared with 14% measured in 1 mM Ca^{2+} (Fig. 3b and Supplementary Fig. 6). As expected, the simulation of SR-95531 also predicted that receptor saturation in trains would be reduced, a result that is entirely dependent on the presence of slow glycine clearance (Supplementary Fig. 4). This modeling approach is limited by a lack of information of the spatial distribution of synapses and their release probabilities. Biological variation in these parameters could explain why IPSC decays vary so widely in different cells. Nevertheless, it is interesting that the IPSC waveforms that we have observed under diverse experimental conditions can be accounted for quantitatively by assuming use-dependent pooling of glycine around granule cells.

Slowing of the decay phase increases effectiveness of inhibition

We explored the physiological importance of the variation in decay time by delivering single and repetitive IPSPs to neurons and determining how long the IPSPs were able to delay resumption of action potential firing. AMPA, NMDA and GABA_A receptor blockers were added to the extracellular solution to isolate glycinergic IPSPs. A continuous depolarizing current injection of 5–10 pA elicited steady action potentials. In response to presynaptic stimuli, IPSPs hyperpolarized the cells and abruptly halted firing (Fig. 7a). On a single IPSP, spikes were inhibited for 192 ± 66 ms (latency from stimulus artifact to first spike, $n = 8$). In contrast, on a train of IPSPs (10 stimuli), the inhibition after the last stimulus was prolonged by over

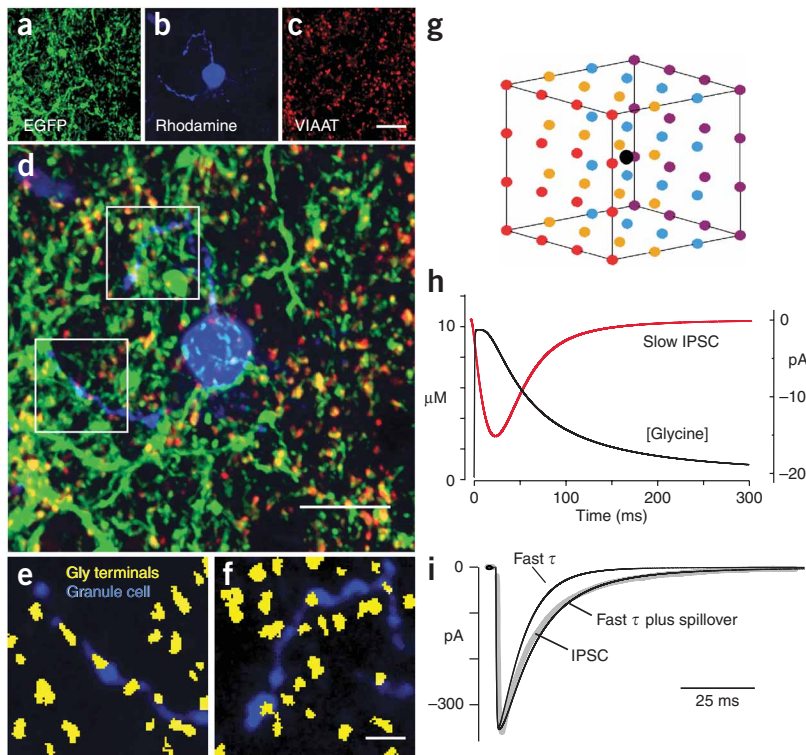


Figure 8 Glycinergic nerve terminal density is consistent with spillover-mediated transmission. (a) EGFP fluorescence in a region of DCN in tissue from a transgenic mouse expressing EGFP in glycinergic neurons. (b) A rhodamine-filled granule cell in the same region as is shown in a. (c) Antibody to VIAAT signal in the same location as in a and b. (d) Merged image of a–c. Regions of overlapping EGFP and VIAAT expression (yellow) were assumed to be glycinergic nerve terminals. (e, f) Sample images used for analysis of glycine nerve terminal density from the lower and upper boxed regions in d, respectively. Yellow regions show colocalized EGFP and VIAAT expression determined by overlaying thresholded EGFP and VIAAT signals (see Methods). The rhodamine-filled granule cell is shown in blue. All images are collapsed stacks of ten adjacent confocal sections acquired 0.2 μm apart in the z axis. Scale bar in c (10 μm) applies to a–c. Scale bar in d represents 10 μm . Scale bar in f (2 μm) applies to e and f. (g) Uniform terminal array in a 10- μm cube. Terminals printed in different colors for clarity. (h) Spillover glycine transient (black) summed over all terminals and measured at cube center (black spot in g). The red trace is the current response to this transient predicted by receptor model. (i) Response of kinetic model (black traces) to fast glycine transient (6 mM peak, 80- μs fast decay, 15 μM peak, 5-ms slow decay), to the sum of the fast transient plus the slow transient in h, and a sample IPSC trace (gray). The weighted time constants of these three traces were 8.7 ms, 15 ms and 15 ms, respectively.

100 ms (326 ± 83 ms from last stimulus artifact to resumption of spikes, $91 \pm 19\%$ increase, $P = 0.0015$, $n = 8$; Fig. 7a–c). Although the extent of the delay varied widely among cells (Fig. 7c), the increase in delay was seen in every case and larger IPSPs tended to produce longer delays (Fig. 7d).

This effect was not the result of recruitment of intrinsic currents by the IPSP, such as A-type K^+ currents, as direct hyperpolarizing current injections of different durations produced spike delays of less than 40 ms, much briefer than those seen with IPSPs (Fig. 7e–h). Moreover, this difference in decay time between single and train IPSPs was not a result of differences in peak synaptic conductance, as demonstrated by examining the duration of spike inhibition with IPSCs of identical duration, but different amplitude (Supplementary Fig. 7 online). Thus, the changes that we have observed in the decay of synaptic currents result in comparable changes in the lifetime of inhibition.

Spillover from glycinergic boutons

Given the magnitude of the spillover component suggested by our data, we asked whether, in principle, the density of glycinergic terminals near

granule cells would predict such a pool of extrasynaptic transmitter. Glycinergic cells were identified in mice expressing green fluorescent protein (GFP) driven by the promoter for GlyT2 (see Supplementary Methods online). Tissue sections were then labeled with an antibody to the GABA/glycine vesicular transporter VIAAT and the convergence of the two labels was used to identify glycinergic boutons (see Methods for complete description of labeling and analysis). This approach proved preferable to labeling with GlyT2 antibodies, as we found that both synaptic and nonsynaptic structures were labeled with a GlyT2 antibody. In the same tissue slice, 2–3 granule cells were labeled by electroporation of a rhodamine-dextran conjugate (Fig. 8a–f). Confocal sections were made of a $10 \times 10 \times 2$ - μm volume containing a granule cell dendrite and we used a thresholding procedure to resolve labeled objects (see Methods). The number of nerve terminals per region was then calculated by dividing the total volume of GFP/VIAAT-positive objects by the median volume of these objects. This approach gave an average terminal density of 0.059 ± 0.021 terminals per μm^3 (6 filled granule cells, 15 regions analyzed, range of 0.027–0.1 terminals per μm^3).

We then simulated diffusion from an array of 512 terminals (sources) arranged uniformly at different densities in the measured range (for 0.08 terminals per μm^3 ; Fig. 8g) and estimated the concentration at a point in the center of the volume (Fig. 8g) over time following exocytosis from the individual sites (ref. 42; see Methods for equation parameters). Summing contributions from all sources gave a glycine transient that rose to 10 μM and decayed over several hundred milliseconds, which should have produced a

small, slow receptor response (Fig. 8h). We then drove our kinetic model of the receptor with a transient representing the sum of the slow spillover component and the large, rapidly decaying transient expected for localized transmission (fast decay phase, 80 μs ; slow phase, 5 ms), as described above. The kinetic model yielded a waveform that was markedly similar in decay time to recorded IPSCs (Fig. 8i). Thus, in principle, glycine spillover adding to local transmission could account for the slow IPSCs in DCN granule cells.

DISCUSSION

The decay of a synaptic response is generally viewed as reflecting the intrinsic gating kinetics of receptors when transmitter clearance is rapid or transmitter rebinding and reactivation of receptors when clearance is slow. Clearance of transmitter is delayed when transmitter pools in or around the synaptic cleft. Some glutamatergic synapses are suited to transmitter pooling by virtue of a high density of synaptic sites⁴³ or an especially broad synaptic cleft⁸. In these cases, however, the effects of pooling are strongly supra-linear in the sense that small increases in stimulus number produces large enhancement and prolongation of

synaptic current and a parallel increase in spiking. Such nonlinearity is optimal for amplification of excitatory signals, but is not well-suited for transmitting graded changes in the level of excitation over a wide range. Our analysis of inhibitory glycinergic transmission revealed an effect on decay that is more linearly related to stimulus number and to the number of quanta released per stimulus. We also observed a very wide range of decay times among cells (\sim tenfold), suggesting that, beyond regulating decay time in an activity-dependent manner, different neurons may have their own set-points for pooling, which are perhaps determined by different densities of nerve terminals. Such a dense glycinergic neuropil is consistent with our analysis and with previous anatomical studies⁴⁴.

Our experiments revealed that multivesicular release affects the amplitude of the IPSC. Distinguishing relative roles for multivesicular release and spillover from adjacent synapses is challenging^{32,45}. We conclude that multivesicular release determines peak IPSC amplitude because the effect of the low-affinity antagonist SR-95531 on peak current was Ca^{2+} dependent, glycine uptake blockers did not change the effectiveness of the antagonist and did not alter the peak amplitude of the IPSC, and larger IPSCs did not rise more slowly than small IPSCs. In contrast, pooling probably sets the decay time because increasing stimulus strength recruited additional fibers and slowed the decay time, increasing stimulus number or frequency slowed the decay time (such slowing was seen at intervals as slow as 50 ms, suggesting that pooling must accumulate transmitter at least over this time frame), SR-95531 shortened the decay time, kinetic models indicated that GlyRs do not generate fast-rising, slowly-decaying IPSCs without a considerable delay in the clearance of transmitter, and the density of glycinergic terminals surrounding granule cells would be expected to generate a substantial spillover component.

Glycinergic synapses vary widely in their decay kinetics. Decay times are extremely fast in most glycinergic synapses of the spinal cord and brainstem, where they presumably solely reflect the biophysical properties of the GlyR. The deactivation time of GlyRs following removal of glycine can be as fast as 4–6 ms^{5,22,39}, although this estimate can be substantially affected by the duration of agonist exposure^{19,40}. As the decay times of glycinergic IPSCs in brainstem and spinal cord are often in the range of 4–6 ms, it is generally thought that deactivation determines the synaptic decay and that glycine clearance must be quite fast. A recent study in spinal cord showed that glycine reached a peak of about 3 mM and cleared the synapse in about 1 ms, resulting in a fast IPSC decay²⁰. Accordingly, in that study, SR-95531 had no effect on the IPSC decay time. For some cases in the auditory system, glycinergic IPSC decays can be even faster^{19,28} as a result of extremely rapid transmitter removal and the action of co-released GABA on the gating of GlyRs¹⁹. In all of these cases, it is likely that fast inhibition allows for effective temporal convergence of signals in a neural circuit.

In contrast, in thalamus, retina and cerebellum, the decay of glycinergic IPSCs, or deactivation of GlyR, can range from 10–40 ms or more^{46–48}. To account for the slow decays seen in auditory granule cells, we initially suspected the expression of a different subtype of synaptic GlyR, and indeed $\alpha 2$ receptors have been associated with slower gating in some cases⁴⁸. This is unlikely in granule cells, however, for several reasons. $\alpha 1$, the most common subsynaptic α subunit, is detected in granule cells, whereas $\alpha 2$ is not⁴⁹. Notably, the effect of subunit composition would probably not be sensitive to quantal content or stimulus intensity, number or frequency; indeed, for quantal currents recorded in Sr^{2+} , synaptic decays were similar to those reported at more classical inhibitory synapses on motor neurons²². The decay time of glycinergic currents in granule cells are similar to those of cerebellar Golgi cells, with

time constants of up to 40 ms⁴⁶, suggesting that the mechanism that we have described may be common to cerebellum-like systems.

The amount of pooled transmitter was graded with the number of axons activated or the number/frequency of stimuli, resulting in progressively slower decays. At the same time, the rise time of IPSCs was constant, consistent with a transmitter time course similar to that used in our model: a rapid and local transient followed by a smaller, slow decay. Trains of slow IPSCs led to steady plateau currents²⁷ and should therefore produce long-lasting changes in the level of inhibition. A similar plateau inhibition with slow decay times has been described at subtypes of GABAergic synapses, but using a very different mechanism¹⁶. There, asynchronous release develops during the stimulus train, smoothing out the current between stimuli and markedly slowing the current decay time. Glycinergic synapses do not appear to be as susceptible to induction of asynchronous release, even at high stimulus rates⁵⁰. Although transmitter pooling permits these synapses to adjust decay times in an activity-dependent manner, an important difference from the GABAergic synapses is that asynchronous release is local to each synapse, whereas pooling would be expected to have effects over larger regions of the cell or even on neighboring cells.

METHODS

Brain slices. Coronal brainstem slices containing the DCN (200 μm) were prepared from Wistar rats (postnatal days 14–25). The care and use of animals was approved by the Institutional Animal Care and Use Committee of Oregon Health and Science University. The rats were anesthetized before decapitation and their brains were removed in warm (35 °C) artificial cerebrospinal fluid that consisted of 125 mM NaCl, 25 mM glucose, 2 mM KCl, 1 mM MgCl_2 , 2 mM CaCl_2 , 1.25 mM NaH_2PO_4 , 26 mM NaHCO_3 , 0.4 mM ascorbic acid, 2 mM sodium pyruvate and 3 mM myo-inositol, bubbled with 5% $\text{CO}_2/95\%$ O_2 (pH 7.4). Slices were then incubated for 25 min in warm artificial cerebrospinal fluid. Recordings were made at 33–35 °C, typically within 4 h of slicing. Neurons were visualized with differential interference contrast microscopy using a 40 \times water-immersion objective.

Electrophysiology. For current clamp, the pipette solution contained 145 mM potassium gluconate, 1 mM MgCl_2 , 10 mM HEPES, 0.2 mM EGTA, 4 mM ATP and 0.3 mM GTP, pH adjusted to 7.3 with KOH. Voltage signals were corrected off-line for a 11-mV junction potential. For voltage clamp, the pipette solution contained 110 mM CsCl, 40 mM HEPES, 2 mM NaCl, 5 mM EGTA, 4 mM magnesium ATP, 0.3 mM sodium GTP, pH adjusted to 7.3 with CsOH. For asynchronous release experiments, 8 mM SrCl_2 replaced CaCl_2 . One set of voltage-clamp experiments testing the effect of low [Cl] on IPSC decay used a pipette solution containing 108 mM CsMeSO_3 , 5 mM CsCl, 1 mM MgCl_2 , 4 mM magnesium ATP, 0.4 mM Tris-ATP, 14 mM Tris-phosphocreatine, 5 mM EGTA, 10 mM HEPES, 3 mM QX-314, pH to 7.3 with CsOH. A 100–200- μs , isolated 5–50 V pulses delivered via an electrode filled with extracellular solution was used to stimulate inhibitory axons. The placement and the stimulus intensity were optimized to obtain the most stable responses. Glycinergic IPSCs were recorded with 10 μM 7-dinitroquinoxaline-2,3-dione, 50 μM DL-2-amino-5-phosphonovaleric acid, 10 μM SR 95531 and 10 μM picrotoxin (in some experiments) at a holding potential of -70 mV. With this solution, all synaptic responses could be completely blocked by the addition of strychnine (0.5 μM , $n = 5$; **Fig. 1c**). Synaptic currents were evoked by extracellular stimulation with a bipolar glass electrode placed ~ 30 – 40 μm away from the granule cell. The currents were recorded with a Multiclamp 700 B amplifier and Clampex software (Molecular Devices).

Analysis. Evoked IPSCs were analyzed in Clampfit 9.2 (Molecular Devices). Aligned IPSCs were averaged and the decays were fit by single or double exponential functions (based on the improvement of the summed square error), $D(t) = A_{\text{FAST}}e^{-t/\tau_{\text{FAST}}} + A_{\text{SLOW}}e^{-t/\tau_{\text{SLOW}}}$, where $D(t)$ is the decay of the mIPSC as a function of time (t), A_{FAST} and A_{SLOW} are constants, and τ_{FAST} and τ_{SLOW} are the fast and slow decay time constants, respectively. In some cases, adding the second exponential component did not substantially decrease

the summed squared error, and so A_{SLOW} was set at 0. The weighted decay time constant was calculated as $\tau_{wd} = (A_{FAST}\tau_{FAST} + A_{SLOW}\tau_{SLOW}) / (A_{FAST} + A_{SLOW})$. Percentage of fast component was calculated as $\%Fast = 100 \times (A_{FAST} / (A_{FAST} + A_{SLOW}))$. For instances in which the decay had more linear components, an equivalent exponential decay time was determined by normalizing the peak to 1 and integrating the entire decay phase. Results are expressed as mean \pm s.e.m. and the significance was determined using Student's paired *t* test (significance indicated by $P < 0.05$, except as indicated).

Kinetic simulations, immunohistochemistry, conductance clamp experiments and diffusion modeling. For details on these experiments, see the **Supplementary Methods**.

Chemicals. DL-2-amino-5-phosphonovaleric acid, 7-dinitroquinoxaline-2,3-dione, 2,3-dihydroxy-6-nitro-7-sulfamoyl-benzo[f]quinoxaline-2,3-dione and SR95531 were obtained from Ascent Scientific. E4CPG, CPPG and CGP-55845 were from Tocris. ORG-25543 a gift from H. Sundaram (Organon Biosciences). All other chemicals were from Sigma. Drugs were dissolved in extracellular solution. In some cases, drugs were first dissolved in DMSO (final DMSO concentration of 0.01%, vol/vol).

Note: Supplementary information is available on the Nature Neuroscience website.

ACKNOWLEDGMENTS

We thank H. Huang, C.E. Jahr and M.E. Roberts for comments on the manuscript and H. Sundaram for the gift of ORG-25543. This work was supported by US National Institutes of Health grant NS028901.

AUTHOR CONTRIBUTIONS

V.B. conducted the electrophysiological experiments, analysis and manuscript preparation. S.P.K. performed immunohistochemistry and analysis. P.D.R. conducted diffusion modeling. L.O.T. conducted kinetic modeling, data analysis and wrote the manuscript.

Published online at <http://www.nature.com/natureneuroscience/>

Reprints and permissions information is available online at <http://www.nature.com/reprintsandpermissions/>

- Katz, B. & Miledi, R. The binding of acetylcholine to receptors and its removal from the synaptic cleft. *J. Physiol. (Lond.)* **231**, 549–574 (1973).
- Barrett, E.F. & Stevens, C.F. The kinetics of transmitter release at the frog neuromuscular junction. *J. Physiol. (Lond.)* **227**, 691–708 (1972).
- Barbour, B., Keller, B.U., Llano, I. & Marty, A. Prolonged presence of glutamate during excitatory synaptic transmission to cerebellar Purkinje cells. *Neuron* **12**, 1331–1343 (1994).
- Jones, M.V. & Westbrook, G.L. Desensitized states prolong GABA_A channel responses to brief agonist pulses. *Neuron* **15**, 181–191 (1995).
- Legendre, P. A reluctant gating mode of glycine receptor channels determines the time course of inhibitory miniature synaptic events in zebrafish hindbrain neurons. *J. Neurosci.* **18**, 2856–2870 (1998).
- Takahashi, T., Momiyama, A., Hirai, K., Hishinuma, F. & Akagi, H. Functional correlation of fetal and adult forms of glycine receptors with developmental changes in inhibitory synaptic receptor channels. *Neuron* **9**, 1155–1161 (1992).
- Otis, T., Zhang, S. & Trussell, L.O. Direct measurement of AMPA receptor desensitization induced by glutamatergic synaptic transmission. *J. Neurosci.* **16**, 7496–7504 (1996).
- Kinney, G.A., Overstreet, L.S. & Slater, N.T. Prolonged physiological entrapment of glutamate in the synaptic cleft of cerebellar unipolar brush cells. *J. Neurophysiol.* **78**, 1320–1333 (1997).
- Otis, T.S., Wu, Y.C. & Trussell, L.O. Delayed clearance of transmitter and the role of glutamate transporters at synapses with multiple release sites. *J. Neurosci.* **16**, 1634–1644 (1996).
- Silver, R.A., Cull-Candy, S.G. & Takahashi, T. Non-NMDA glutamate receptor occupancy and open probability at a rat cerebellar synapse with single and multiple release sites. *J. Physiol. (Lond.)* **494**, 231–250 (1996).
- Kondo, S. & Marty, A. Synaptic currents at individual connections among stellate cells in rat cerebellar slices. *J. Physiol. (Lond.)* **509**, 221–232 (1998).
- Biro, A.A., Holderith, N.B. & Nusser, Z. Release probability-dependent scaling of the postsynaptic responses at single hippocampal GABAergic synapses. *J. Neurosci.* **26**, 12487–12496 (2006).
- Cathala, L., Holderith, N.B., Nusser, Z., DiGregorio, D.A. & Cull-Candy, S.G. Changes in synaptic structure underlie the developmental speeding of AMPA receptor-mediated EPSCs. *Nat. Neurosci.* **8**, 1310–1318 (2005).
- Isaacson, J.S., Solis, J.M. & Nicoll, R.A. Local and diffuse synaptic actions of GABA in the hippocampus. *Neuron* **10**, 165–175 (1993).
- Banks, M.I., Li, T.B. & Pearce, R.A. The synaptic basis of GABA_A,slow. *J. Neurosci.* **18**, 1305–1317 (1998).
- Lu, T. & Trussell, L.O. Inhibitory transmission mediated by asynchronous transmitter release. *Neuron* **26**, 683–694 (2000).
- Legendre, P. The glycinergic inhibitory synapse. *Cell. Mol. Life Sci.* **58**, 760–793 (2001).
- Burzomato, V., Beato, M., Groot-Kormelink, P.J., Colquhoun, D. & Sivilotti, L.G. Single-channel behavior of heteromeric alpha1beta glycine receptors: an attempt to detect a conformational change before the channel opens. *J. Neurosci.* **24**, 10924–10940 (2004).
- Lu, T., Rubio, M.E. & Trussell, L.O. Glycinergic transmission shaped by the co-release of GABA in a mammalian auditory synapse. *Neuron* **57**, 524–535 (2008).
- Beato, M. The time course of transmitter at glycinergic synapses onto motoneurons. *J. Neurosci.* **28**, 7412–7425 (2008).
- Brand, A., Behrend, O., Marquardt, T., McAlpine, D. & Grothe, B. Precise inhibition is essential for microsecond interaural time difference coding. *Nature* **417**, 543–547 (2002).
- Singer, J.H. & Berger, A.J. Contribution of single-channel properties to the time course and amplitude variance of quantal glycine currents recorded in rat motoneurons. *J. Neurophysiol.* **81**, 1608–1616 (1999).
- Harty, T.P. & Manis, P.B. Kinetic analysis of glycine receptor currents in ventral cochlear nucleus. *J. Neurophysiol.* **79**, 1891–1901 (1998).
- Mager, S. et al. Steady states, charge movements and rates for a cloned GABA transporter expressed in *Xenopus* oocytes. *Neuron* **10**, 177–188 (1993).
- Wadiche, J.I., Arriza, J.L., Amara, S.G. & Kavanaugh, M.P. Kinetics of a human glutamate transporter. *Neuron* **14**, 1019–1027 (1995).
- Oertel, D. & Young, E.D. What's a cerebellar circuit doing in the auditory system? *Trends Neurosci.* **27**, 104–110 (2004).
- Balakrishnan, V. & Trussell, L.O. Synaptic inputs to granule cells of the dorsal cochlear nucleus. *J. Neurophysiol.* **99**, 208–219 (2008).
- Awatramani, G.B., Turecek, R. & Trussell, L.O. Inhibitory control at a synaptic relay. *J. Neurosci.* **24**, 2643–2647 (2004).
- Magnusson, A.K., Kapfer, C., Grothe, B. & Koch, U. Maturation of glycinergic inhibition in the gerbil medial superior olive after hearing onset. *J. Physiol. (Lond.)* **568**, 497–512 (2005).
- Silver, R.A., Traynelis, S.F. & Cull-Candy, S.G. Rapid time course miniature and evoked excitatory currents at cerebellar synapses in situ. *Nature* **355**, 163–166 (1992).
- Pitt, S.J., Sivilotti, L.G. & Beato, M. High intracellular chloride slows the decay of glycinergic currents. *J. Neurosci.* **28**, 11454–11467 (2008).
- Christie, J.M. & Jahr, C.E. Multivesicular release at Schaffer collateral-CA1 hippocampal synapses. *J. Neurosci.* **26**, 210–216 (2006).
- Tong, G. & Jahr, C.E. Block of glutamate transporters potentiates postsynaptic excitation. *Neuron* **13**, 1195–1203 (1994).
- Atkinson, B.N. et al. ALX 5407: a potent, selective inhibitor of the hGlyT1 glycine transporter. *Mol. Pharmacol.* **60**, 1414–1420 (2001).
- Whitehead, K.J. et al. Positive N-methyl-D-aspartate receptor modulation by selective glycine transporter-1 inhibition in the rat dorsal spinal cord *in vivo*. *Neuroscience* **126**, 381–390 (2004).
- Beato, M., Burzomato, V. & Sivilotti, L.G. The kinetics of inhibition of rat recombinant heteromeric alpha1beta glycine receptors by the low-affinity antagonist SR-95531. *J. Physiol. (Lond.)* **580**, 171–179 (2007).
- Wang, P. & Slaughter, M.M. Effects of GABA receptor antagonists on retinal glycine receptors and on homomeric glycine receptor alpha subunits. *J. Neurophysiol.* **93**, 3120–3126 (2005).
- Fucile, S., de Saint Jan, D., David-Watine, B., Korn, H. & Bregestovski, P. Comparison of glycine and GABA actions on the zebrafish homomeric glycine receptor. *J. Physiol. (Lond.)* **517**, 369–383 (1999).
- Genet, L.J. & Clements, J.D. Binding site stoichiometry and the effects of phosphorylation on human alpha1 homomeric glycine receptors. *J. Physiol. (Lond.)* **544**, 97–106 (2002).
- Mohammadi, B. et al. Kinetic analysis of recombinant mammalian alpha(1) and alpha(1)beta glycine receptor channels. *Eur. Biophys. J.* **32**, 529–536 (2003).
- Twyman, R.E. & Macdonald, R.L. Kinetic properties of the glycine receptor main- and sub-conductance states of mouse spinal cord neurones in culture. *J. Physiol. (Lond.)* **435**, 303–331 (1991).
- Barbour, B. & Hausser, M. Intersynaptic diffusion of neurotransmitter. *Trends Neurosci.* **20**, 377–384 (1997).
- Carter, A.G. & Regehr, W.G. Prolonged synaptic currents and glutamate spillover at the parallel fiber to stellate cell synapse. *J. Neurosci.* **20**, 4423–4434 (2000).
- Alibardi, L. Ultrastructural distribution of glycinergic and GABAergic neurons and axon terminals in the rat dorsal cochlear nucleus, with emphasis on granule cell areas. *J. Anat.* **203**, 31–56 (2003).
- Wadiche, J.I. & Jahr, C.E. Multivesicular release at climbing fiber–Purkinje cell synapses. *Neuron* **32**, 301–313 (2001).
- Dumoulin, A., Triller, A. & Dieudonne, S. IPSC kinetics at identified GABAergic and mixed GABAergic and glycinergic synapses onto cerebellar Golgi cells. *J. Neurosci.* **21**, 6045–6057 (2001).
- Kraushaar, U. & Backus, K.H. Characterization of GABA(A) and glycine receptors in neurons of the developing rat inferior colliculus. *Pflugers Arch.* **445**, 279–288 (2002).
- Veruki, M.L., Gill, S.B. & Hartveit, E. Spontaneous IPSCs and glycine receptors with slow kinetics in wide-field amacrine cells in the mature rat retina. *J. Physiol. (Lond.)* **581**, 203–219 (2007).
- Piechotta, K., Weth, F., Harvey, R.J. & Friauf, E. Localization of rat glycine receptor alpha1 and alpha2 subunit transcripts in the developing auditory brainstem. *J. Comp. Neurol.* **438**, 336–352 (2001).
- Awatramani, G.B., Turecek, R. & Trussell, L.O. Staggered development of GABAergic and glycinergic transmission in the MNTB. *J. Neurophysiol.* **93**, 819–828 (2005).

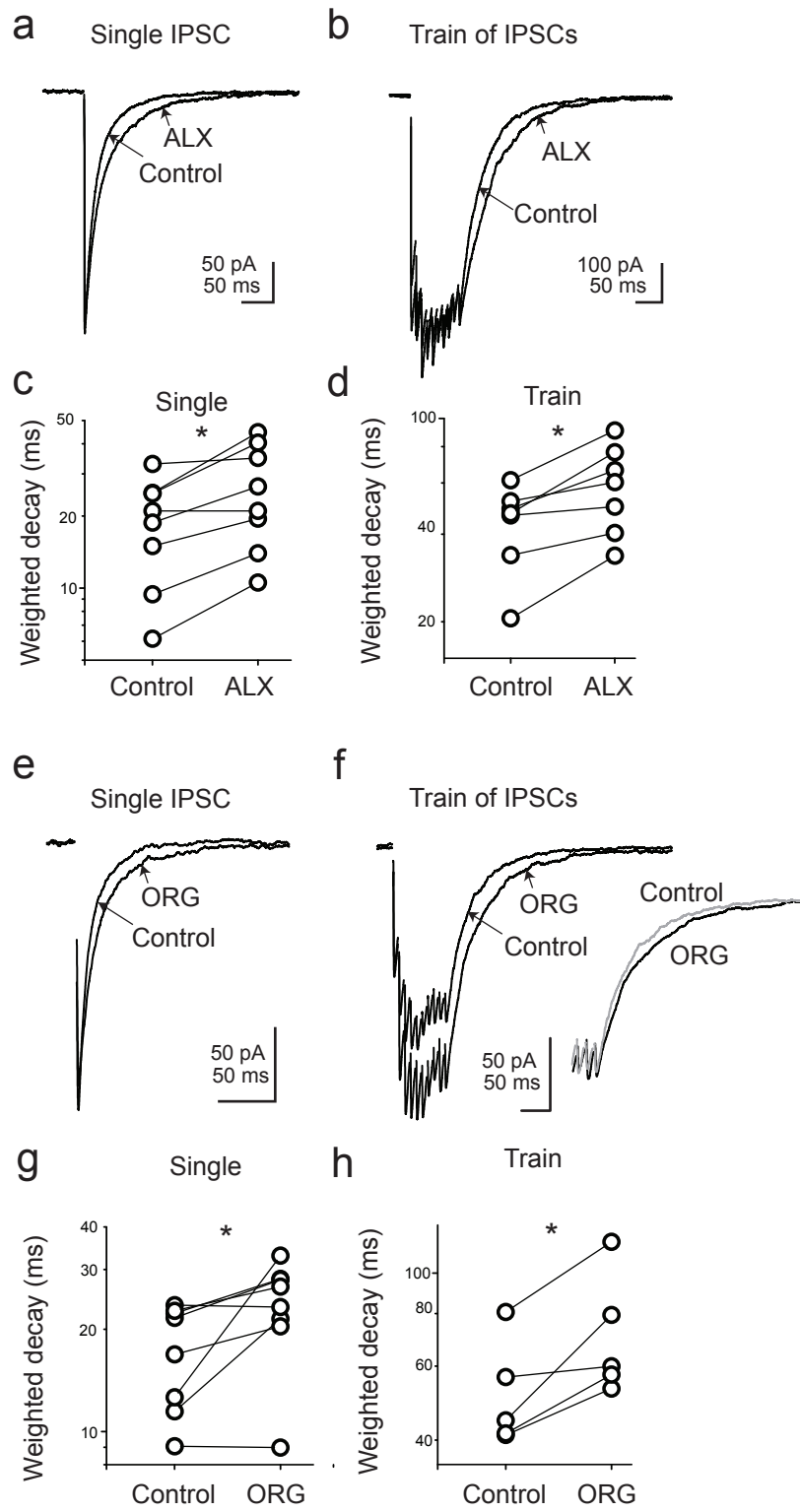


Fig.S1

Figure S1 Glial transporter regulate the IPSC decay time. (a) Averaged traces of glycinergic IPSC under control condition and in the presence of ALX-5407 (“ALX”, 20 μ M), upon single synaptic stimulation. The weighted decay time was 25 ms in the control and 40 ms in the presence of ALX-5407. (b) Response to 10 stimuli at 100 Hz under control condition and in the presence of ALX-5407. The weighted decay time was 49 ms in the control and 66 ms in the presence of ALX-5407. (c & d) Plot of weighted decay constants of glycinergic IPSCs from individual cells in control condition and in the presence of ALX, upon single and train synaptic stimulations. The weighted decay constants were significantly slowed upon ALX application with single (n=8; $P < 0.02$) and train (n=7; $P < 0.008$) of stimulation. (e) Averaged traces of glycinergic IPSC under control condition and in the presence of ORG-25543 (“ORG”, 20 μ M), upon single synaptic stimulation. The weighted decay time was 11.5 ms in the control and 21.4 ms in the presence of ORG-25543. (f) Response to 10 stimuli at 100 Hz under control condition and in the presence of ORG-25543. The weighted decay time was 41.2 ms in the control and 53.0 ms in the presence of ORG-25543. (g & h) Plot of weighted decay constants of glycinergic IPSCs from individual cells in control condition and in the presence of ORG-25543 upon single and train synaptic stimulations. The weighted decay constants were significantly slowed upon ORG-25543 application with single (n=8; $P < 0.03$) and train (n=5; $P < 0.04$) of stimulation.

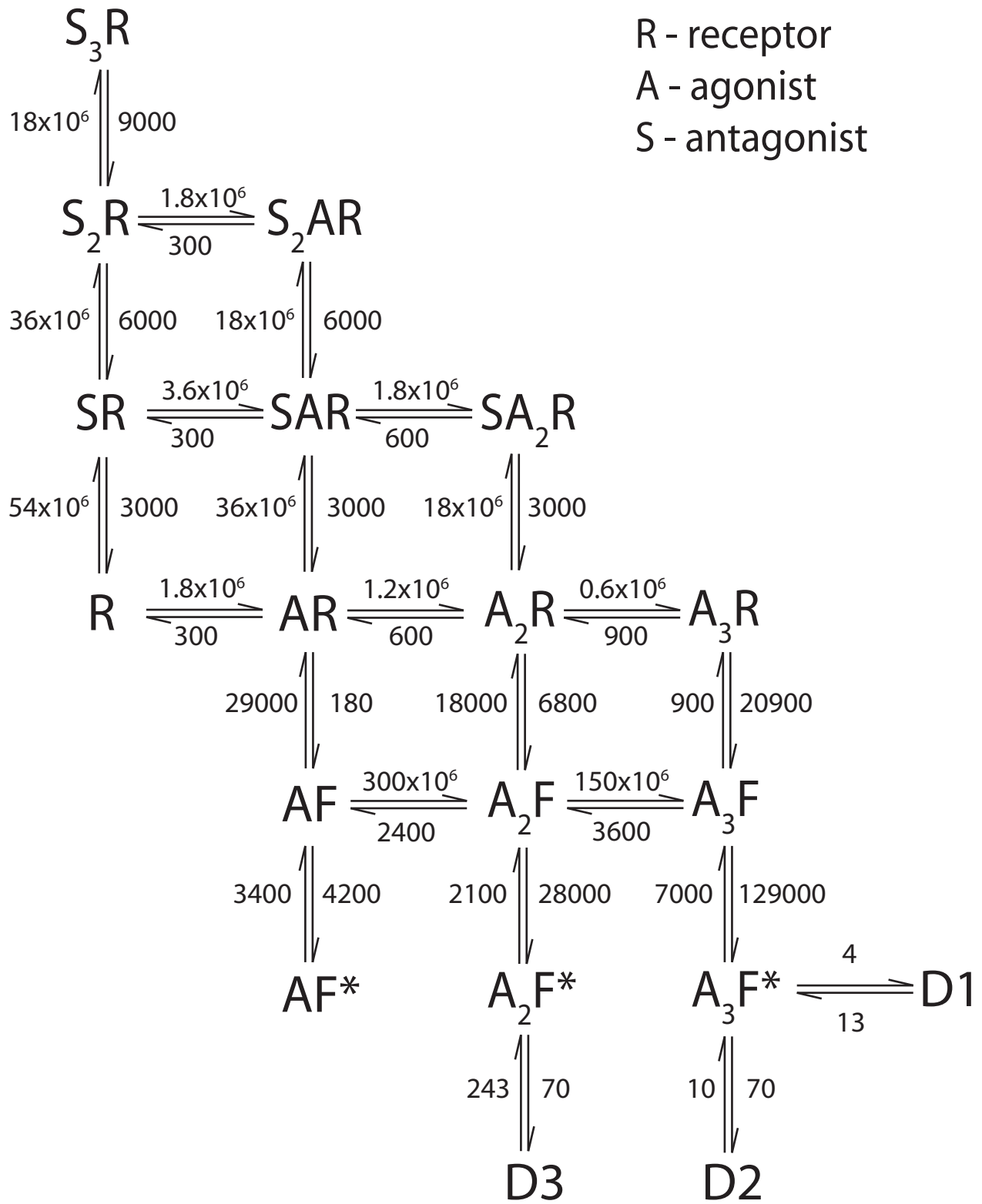


Fig S2

Figure S2

Kinetic model of heteromeric GlyR channel gating ¹ was modified in two respects. First, desensitized states were added to account for desensitization of macroscopic currents (M. Beato, pers. comm.). Second, the interaction of the receptor with the antagonist SR-95531 was included, according to the rate constants determined in ⁶. Units are 1/s except for ligand binding steps (1/M.s). A: agonist (glycine). S: antagonist (SR-95531).

R: receptor.

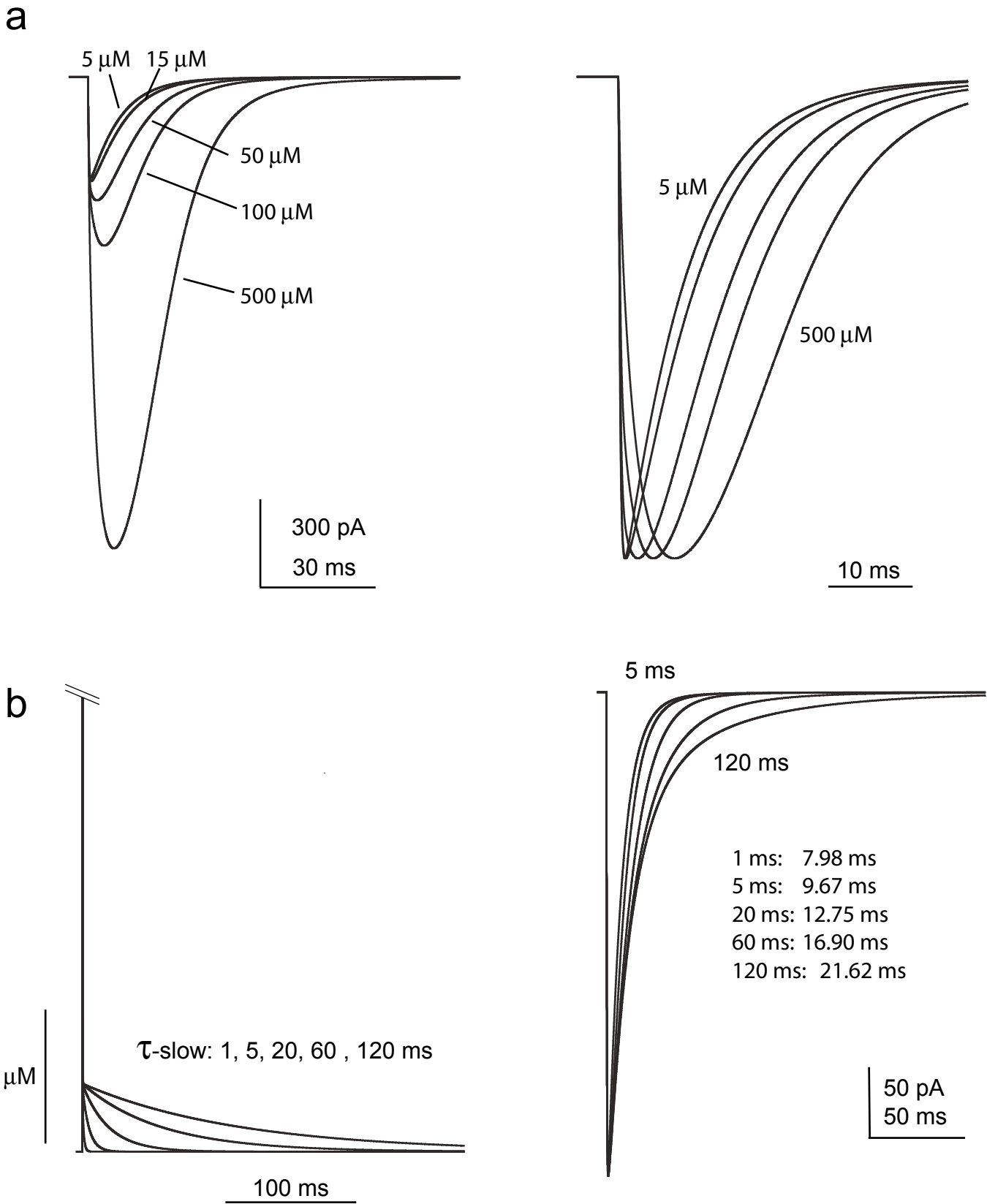


Fig. S3

Figure S3 Simulations of glycinergic IPSCs. (a) Simulations of receptor model using a transmitter transient with a peak of 6 mM, fast decay of 80 μ s, followed by a 5 ms slow decay phase whose amplitude is indicated in the panel. Increasing the small slow component both increased the amplitude and slowed the rising phase (shown normalized on right). 10-90% rise times are 0.35 ms (5 μ M), 0.38 ms (15 μ M), 0.61 ms (50 μ M), 1.71 ms (100 μ M), 3.25 ms (500 μ M). (b) The transmitter transient in which the 15 μ M slow component was varied as indicated. On the right are resulting receptor simulations for each of these five transients. IPSC decay times associated with each are indicated in the table.

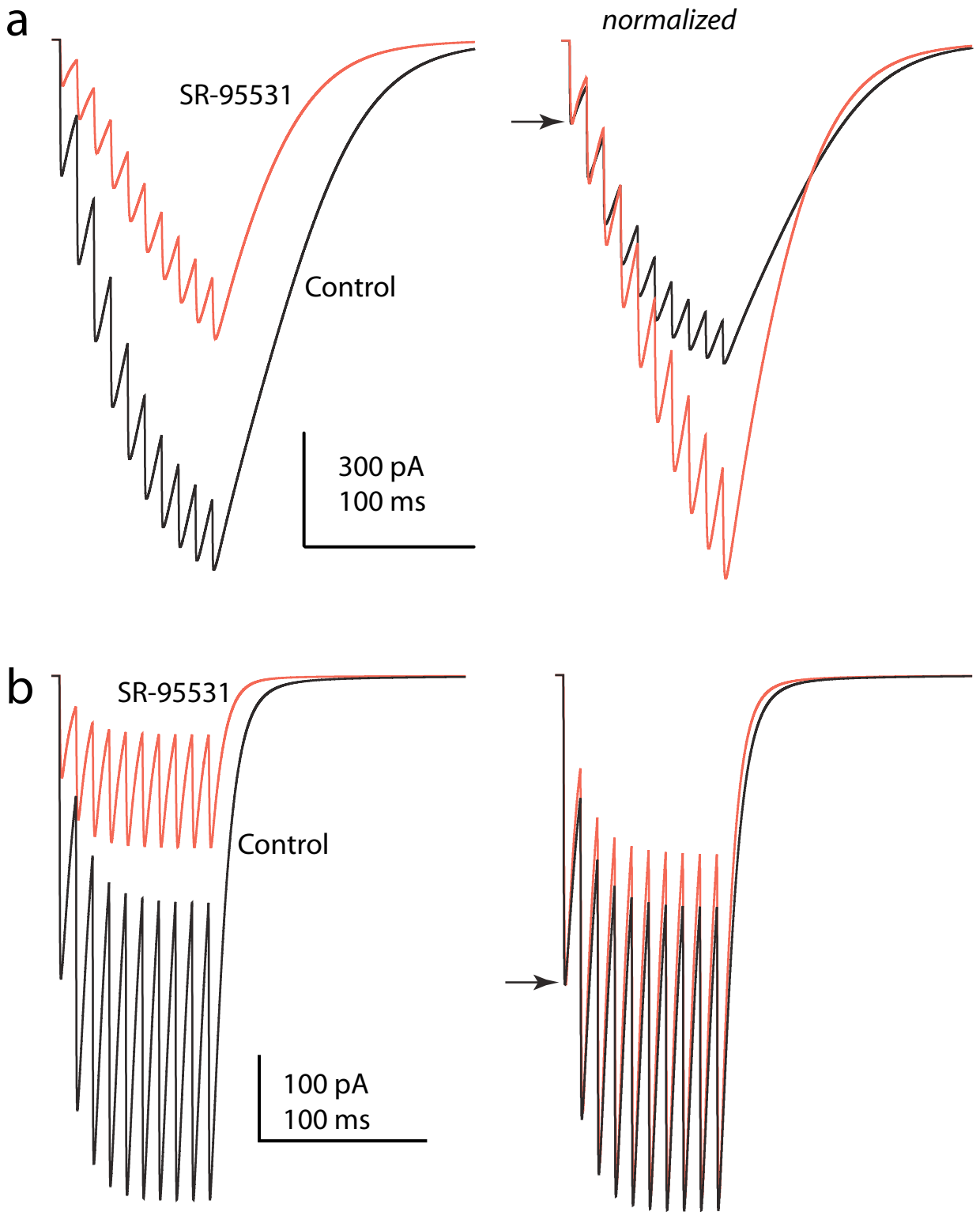


Fig.S4

Figure S4 Simulations of receptor responses to 10 glycine transients delivered at 100 Hz, with and without modeling interactions of 300 μ M SR-95531. (a) uses a 60-ms slow glycine decay component while (b) uses a 5-ms component. On right of each panel, the traces are normalized to the amplitude of the first IPSC (indicated by arrow).

Nature Neuroscience: doi:10.1038/nn.2265

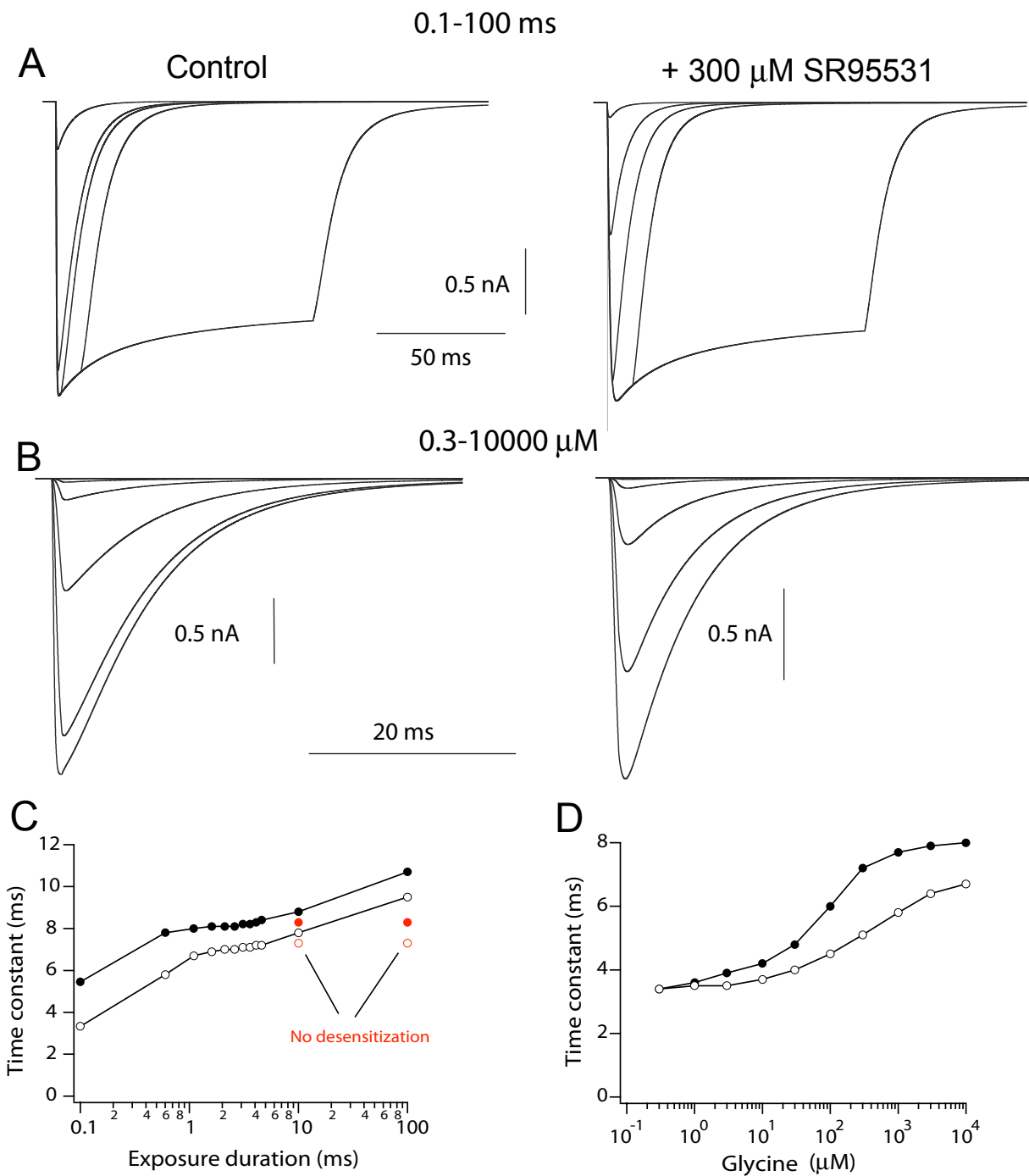


Fig.S5

Figure S5 Simulations using square pulses of glycine at the indicated durations (using 6 mM glycine) and durations (using 1-ms pulses). Righthand panels in A and B include 300 μ M SR-95531 in control and glycine. C, Weighted time constant of deactivation from simulated currents vs pulse duration. Filled symbols: control. Open symbols: + SR-95531. Red symbols, entry into desensitization set to zero. D, Weighted time constant of deactivation from simulated currents vs pulse concentration. Filled symbols: control. Open symbols: + SR-95531.

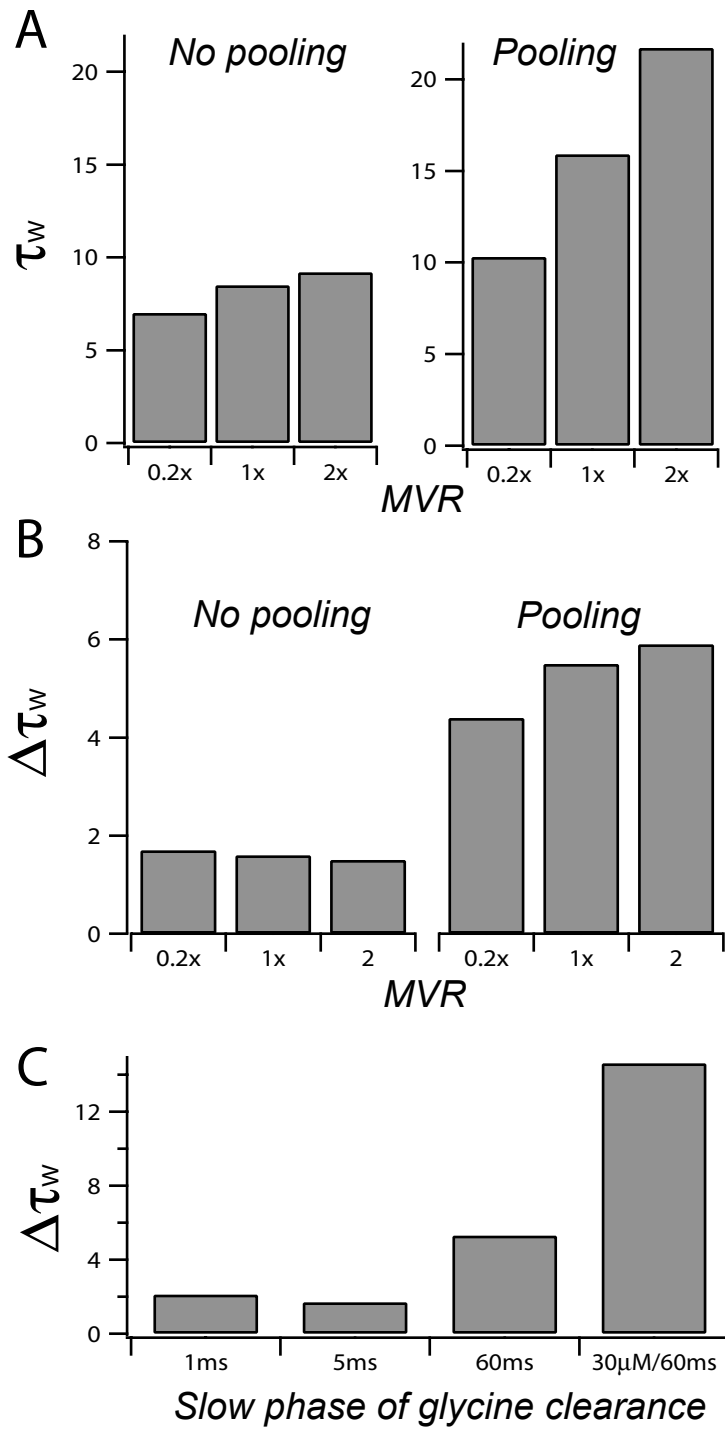


Fig.S6

Figure S6 Decay time constant of simulated IPSCs varying transmitter transients and antagonist. A, multivesicular release (MVR) was varied by scaling the peak concentrations from 6 mM (1x) to 1.2 mM (0.2x) and 12 mM (2x). Pooling was modeled by increasing the slow phase of glycine clearance from 5 ms (no pooling) to 60 ms (pooling). Weighted time constant (τ_w) determined from simulations either by weighting components of a biexponential fit, or normalizing the peak current and integrating the decay phase. The latter was used when the decay was clearly not exponential (e.g., contained a linear component). Experimentally determined current decays ranged from 6 to 60 ms, with a mean of 22 ms. B, Predicted difference in decay time constant between control and in SR-95531 given variation in pooling and MVR. The experimentally determined difference was 6 ms. C, Predicted difference in decay time constant as in B, with variation in lifetime of the slow phase of clearance. 1-60 ms time constants had a starting amplitude of 15 μ M. Also simulated was a trial with 30 μ M and 60 ms. Larger concentrations distorted the rise time of the IPSC.

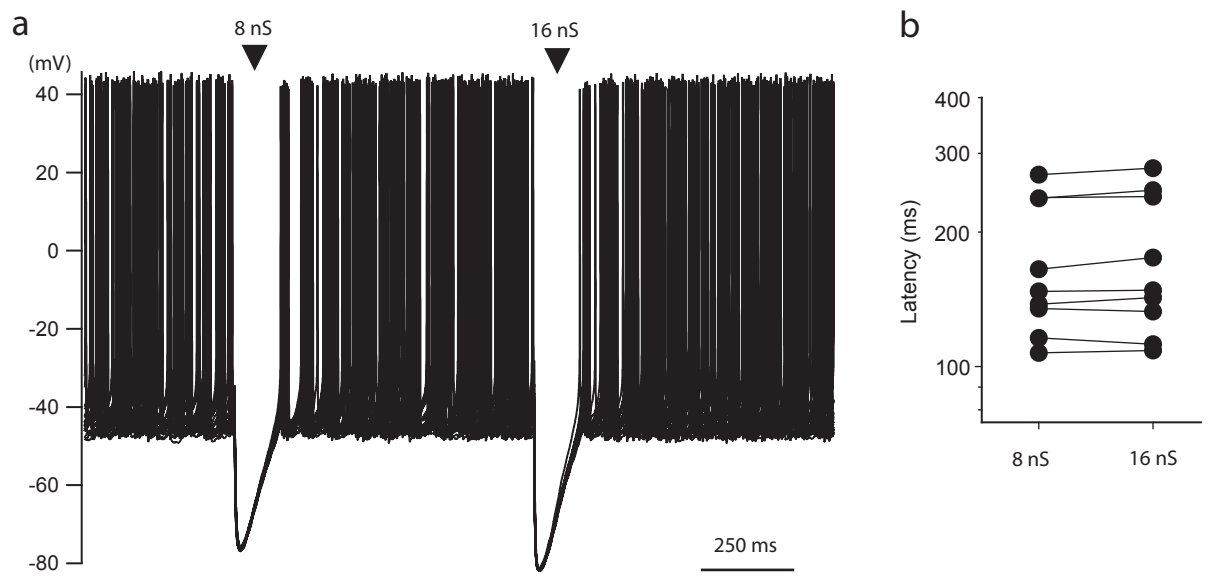


Fig.S7

Figure S7. Varying IPSPG amplitude over physiological range does not contribute to the duration of inhibition. (a) Example traces showing the duration of spike inhibition following 8 and 16 nS IPSPGs. The kinetics of the injected IPSPGs were based on recorded IPSCs (decay time constant = 15 ms and 10–90% rise time = 0.3 ms). Arrowheads indicate corresponding injected IPSPG. (b) The latency period between the time of the start of IPSPG injection and resumption of action potential firing was calculated as in Fig 8. Latency before spiking resumption did not differ significantly with 8 and 16 nS IPSPG injection. Mean latency for 8 nS: 172.7 ± 19.9 ms; for 16 nS: 176.2 ± 21.1 (n=9 cells, p=0.08).

SUPPLEMENTAL METHODS

Estimation of glycine nerve terminal density. Terminal density was estimated using confocal stereology of regions labeled for glycinergic markers surrounding individual marked granule cells (see Supplemental Methods). Slices of auditory brainstem (200 μm thick) were prepared from mice (P18) expressing enhanced green fluorescent protein under control of the neuronal glycine transporter GlyT2¹¹ as described above and granule cells in the fusiform cell layer of DCN or the granule cell area between DCN and VCN were filled with dye by electroporation. A micropipette filled with anionic rhodamine-dextran (10% in internal solution; 3000 MW; Molecular Probes) was placed just above a granule cell, and a brief train of square wave pulses was applied to the pipette (50V, 3-5 pulses, 50 ms duration, 10 Hz) using a stimulus isolator (AMPI; Jerusalem, Israel). A 15-30 minute incubation period was used to ensure loading of dendrites. After loading, slices were fixed by 10 minute incubation in 4% formaldehyde in 0.1 M phosphate-buffered saline (PBS). The tissue was then washed extensively in PBS and stored overnight at 4°C in 30% sucrose in PBS. The following day, slices were rinsed in PBS and immersed for 1 hour at room temperature in a blocking solution containing 2% normal goat serum, 3% bovine serum albumin, and 0.2% Triton X-100 in PBS. Slices were subsequently incubated overnight at 4°C with an antibody directed against the vesicular inhibitory amino acid transporter (rabbit anti-VIAAT; diluted 1:2000 in blocking solution; Synaptic Systems; Goettingen, Germany). After primary antibody incubation, the tissue was washed and exposed to goat anti-rabbit secondary antibody conjugated to Alexa Fluor 633 (1:200 in block solution without Triton X-100; Invitrogen; Carlsbad, CA). Tissue was mounted on slides, dehydrated in ascending alcohols,

delipidized in xylenes, rehydrated, and coverslipped using Fluoromount G medium (Southern Biotech; Birmingham, AL). Fluorescence from EGFP, rhodamine and Alexa Fluor 633 was imaged sequentially on a confocal microscope (Olympus, FV1000) at 60x magnification using an oil-immersion objective (N.A. 1.42) and 2.0X digital zoom.

Image analysis was performed using ImageJ software (NIH; Bethesda, MD). To enhance the edges of fluorescent objects, a local unsharp masking procedure was applied individually to EGFP and Alexa Fluor 633 fluorescence images; images were median filtered with a radius of 7 pixels (~0.7 μm) and this filtered representation was subsequently subtracted from the original fluorescence image. In addition to helping resolve the boundaries of fluorescent puncta, this method improved detection of EGFP and VIAAT signals across the entire range of fluorescence levels by increasing contrast according to local pixel intensities. Co-localization of EGFP and VIAAT was determined by assessing overlap between EGFP and Alexa Fluor 633 signals after separately thresholding fluorescence from the two channels visually and applying a binary mask to the thresholded images. Regions of interest (ROIs) that extended 10 μm in the X and Y directions and 2 μm in the Z-axis were selected around dendritic and somatodendritic regions of dye-filled granule cells and overlapping regions of EGFP and VIAAT expression larger than 0.047 μm^3 (i.e., larger than the mean \pm 2SD volume of overlapping EGFP and Alexa Fluor 633 signals in no-primary control tissue), were detected within the ROIs using the 3D Object Counter plug-in for ImageJ (F. Cordelires, J. Jackson; <http://rsbweb.nih.gov/ij/plugins/track/objects.html>) (15 regions around 6 dye-filled cells analyzed). The total volume of the detected EGFP/Alexa Fluor 633-positive

objects was divided by the median volume of these objects (mean \pm SD=0.155 \pm 0.037 μm^3) to yield an estimate of the number of glycinergic nerve terminals within the region of interest. Glycinergic nerve terminal density values were corrected for a z-axis tissue shrinkage factor of 63.1 \pm 6.8% determined by measuring tissue thickness prior to and after fixation and dehydration (n=3 slices).

Diffusion modeling: To estimate the profile of glycine concentration transients near synapses, we applied a model of spillover of transmitter from multiple sources using the linear solution to 3-dimensional diffusion in a porous medium ¹². A grid of release sites was modeled based on the measured densities and a total of 512 sites; this corresponded to a modeled cubic volume of 18.6 μm per side. The glycine concentration transient at the center of the cube, $G(t)$, was calculated by the superposition of diffusion solutions from all the release sites, $G(t) = \sum_i g(r_i, t)$, where $g(r, t)$ was the glycine concentration transient caused by release at site i , a distance or r_i μm from the center of the cube. The solutions for diffusion in a porous medium were given by ¹²,

$$g(r_i, t) = \frac{M}{\alpha(\pi(4D/\lambda^2)t)^{3/2}} \exp\left[\frac{-r_i^2}{(4D/\lambda^2)t}\right]$$

where M was the number of molecules released at each site (assuming 5000 molecules per vesicle and a release of 2-4 vesicles per terminal (varied randomly among terminals) to account for multivesicular release), $D=1.33 \times 10^{-5}$ ($\text{cm}^2 \text{s}^{-1}$) was the free diffusion coefficient for glycine corrected for temperature, $\alpha=0.21$ was the volume fraction, and $\lambda=1.77$ was the tortuosity. The values for α and λ were consistent with the

range proposed for cerebellar slice preparations¹³. Numerical results were calculated using custom scripts in Matlab R2007b (The Mathworks) . For simplicity, uptake was not modeled, given the rather modest effects of uptake block on IPSCs and the lack of information about uptake rates (Fig S1).

Conductance-clamp experiments: Simulated inhibitory conductances (IPSGs) were scaled by V_M and E_{CHLORIDE} with an SM-1 amplifier (Cambridge Conductance, Cambridge, UK), and the resulting dynamic current waveform injected into granule cells. The Cl^- reversal potential, estimated for the K-gluconate intracellular solution, was set to -80 mV. A liquid junction potential of -13 mV was subtracted on line. The kinetics of the injected IPSGs (8 and 16 nS peak conductance) were based on recorded IPSCs (decay time constant= 15 ms and 10–90% rise time= 0.3 ms).

SUPPLEMENTAL RESULTS

Kinetic modeling.

General observations. Several kinetic models of GlyRs are available, each optimized to explore distinct aspects of gating¹⁻³. These predict relatively rapid deactivation and, over brief time periods, rather incomplete desensitization. We used the recent model of Burzomato et al.¹, which was developed to account accurately for single heteromeric glycine channel kinetics in cell-attached patches. The authors have modified their original scheme to include desensitization (Marco Beato, pers. comm.), and these rates were then adjusted to account for the somewhat slower desensitization seen in auditory neurons (⁴; Tao Lu, unpublished obs.). Figure S2 shows their model as implemented here and the associated rate constants. Except for desensitization, none of the rates were altered from their model, as an attempt to restrict ourselves solely to the question of how the glycine concentration waveform could account for our results. To simulate currents, we used 1000 channels of 40 pS each⁵ and a driving force of -60 mV. The model was modified to account for the actions of the antagonist SR-95531, using the scheme presented by Beato et al.⁶, who measured the rates associated with SR-95531 binding and unbinding from heteromeric GlyRs. In the model, each glycine binding site could be occupied by an antagonist molecule; however for simplicity we assumed that the “flip” state in Burzomato et al.’s model (which precedes channel opening) could not bind antagonist. The model was implemented using Axograph 1.0 software, and predicted an EC50 of 80 μ M, and Hill coefficient of 1.8 when tested with long pulses of

agonist. 300 μM SR-95531 shifted the EC50 to the right (EC50 186 μM , Hill coefficient 1.8), as shown experimentally ⁶.

Using this model, we then explored transmitter transients that could account for IPSCs in granule cells. Transmitter diffusion from single sites has been extensively modeled using either sums of exponential decays, analytical solutions to diffusion equations, or stochastic modeling of diffusion. All have a common element of a rapid fall-off from mM levels near the release site over a period of a few 100 μs , followed by a small, slower phase of decay. This second phase of decay varies depending on assumptions of the particular model (e.g., diffusion within a plane vs a volume or the level of ‘tortuosity’ of the diffusion path), but typically falls off over 1-5 ms.

Inhibitory synapses onto granule cells are most likely conventional bouton-like structures; although large “mossy” endings with pleomorphic vesicles have been described, these are relatively uncommon (⁷; D. Ryugo, Pers. Comm.), and thus there is little reason to suspect restricted diffusion of glycine. We therefore assumed that slow clearance of glycine must result from pooling among a population of inhibitory synapses. Thus the slowed IPSC would be a consequence of slowing of the late phase of transmitter decay at each synapse.

Multiple sets of simulations were conducted to explore the importance of specific parameters. The peak glycine transient was varied between 3-12 mM. At 6 mM (80 μs decay) the peak open probability was 15%. Although the peak open probability during

IPSCs based on fluctuation measurements is between 0.4-0.5^{8,9}, we opted for the lower value in order to account for summation of currents during high frequency trains and to give greater freedom to explore consequences of multivesicular release. The relatively low EC50 and low desensitization of GlyRs led to several restrictions on the duration and amplitude of the concentration transient. Fig S3a shows the effect of varying the amplitude of the slow phase of glycine decay between 5-500 μM with a 5 ms decay time. A value of about 500 μM was previously used to model successfully the slow phase of decay of glutamate at cerebellar synapses. However, in the GlyR model this level enhanced and slowed the peak dramatically. Only values less than 20 μM gave rise times under 0.4 ms, our target level for matching IPSCs (Fig 1f). At 5 μM , summation of slow current during trains was minimized, while 15 μM gave a decay time consistent with the middle range of experimental values. The slow decay time was varied between 1-120 ms (Fig S3b), and showed clearly that grading this parameter could account for variation in the decay phase of granule cell IPSCs.

Competitive antagonist action. In addition to the model predictions shown in Fig 7, we also explored how the model would describe the effects of SR-95531 on train stimuli, under conditions in which the slow phase of glycine decay is set to either 5 ms or 60 ms in Fig S4. Comparing panels Fig S4a and Fig S4b highlights that the decay after trains is sharply dependent on the presence of slow phase of glycine clearance. The decay after a train in control solutions was increased 3 fold over the single-stimulus decay; by contrast, using the faster glycine clearance, the train decayed only 1.14 fold slower (Fig S4b). In the presence of SR-95531, all IPSCs in a train were reduced, but the ratio of

initial to late IPSC amplitudes was less affected by SR-95531 when the slow glycine transient was reduced from 60 ms to 5 ms. For example, using the 60 ms decay comparing the amplitude of IPSC 10 to IPSC 1 as in Fig 5d, the ratio was 0.55 for control and 1.37 with SR-95531, a difference within the range of our experimental results (Fig 5d). When using the 5 ms glycine decay the ratios were 0.98 and 1.10 respectively. Together, these simulation highlight the absolute requirement for a slow clearance of glycine from the synaptic cleft to account for our experimental data.

Dose- and duration-response relations. The analysis of Burzomato et al (2004), and others¹⁰ predicts several unusual features of the GlyR, including a dependence of the current decay on both the peak glycine concentration and glycine exposure time. We therefore asked what is the range of these effects, how do they impact our conclusions about the transmitter lifetime, and how would SR-95531 be expected to alter the relation between these parameters. Fig. S5 shows a set of simulations using square pulses of glycine with and without 300 μ M of the low affinity antagonist. In Fig. S5a, pulses of 6 mM glycine ranged in duration from 0.1 to 100 ms; the weighted deactivation time constants are shown in Fig S5c (filled symbols). These show that increasing exposure time increases deactivation from about 5.5 to 10 ms. The initial phase of increase reflects the gating of longer lived open states, while the second phase of increase is due to desensitization. In either case, it is clear that changes in deactivation by prolonged exposure cannot account for the decay of the evoked IPSCs. In Fig S5b a 1-ms pulses is delivered at concentrations ranging from 0.3-10,000 μ M, and the resulting dose-response curve is in Fig S5d (filled symbols). While the decay times could range from

about 3.5 to 8 ms, they were still far briefer than that of evoked synaptic currents in DCN granule cells.

MVR versus Pooling. Simulations using a combination of changes in peak cleft concentrations (multivesicular release), pooling (slow phase of transmitter clearance) and the presence of a low-affinity antagonist allowed us to gain stronger evidence in favor of glycine pooling. Fig S6a shows the weighted decay of currents in which the peak concentration was increased or decreased from our standard level of 6 mM, encompassing a 10-fold range. In each of these, the duration of the slow phase of clearance was set to 5 or 60 ms. The results show that without pooling, MVR cannot account for the synaptic decay time which in a set of 33 cells, averaged 22 ± 2 ms (range 6-60 ms). We then explored the effect of the antagonist on this relation. In Fig S5c,d we show that the antagonist is expected to shorten the decay time of the IPSC (open circles), probably by preventing reopening of receptors in singly or doubly ligated states. However the absolute magnitude of this effect is much smaller than that seen with IPSCs (6 ms). In Fig S6b we tested the difference in time constant with and without antagonist. Varying pooling and multivesicular release as described above. Again, only by assuming transmitter pooling could we reach an effect similar to that seen experimentally. In Fig S6c, we varied the slow phase of clearance from 1 ms to 60 ms, and also altered its magnitude from 15 μ M to 30 μ M. Again, the magnitude of the effect of the antagonist on decay time was only reproduced with very slow transmitter clearance times.

1. Burzomato, V., Beato, M., Groot-Kormelink, P.J., Colquhoun, D. & Sivilotti, L.G. Single-channel behavior of heteromeric alpha1beta glycine receptors: an attempt to detect a conformational change before the channel opens. *J Neurosci* **24**, 10924-10940 (2004).
2. Gentet, L.J. & Clements, J.D. Binding site stoichiometry and the effects of phosphorylation on human alpha1 homomeric glycine receptors. *J Physiol* **544**, 97-106 (2002).
3. Legendre, P. A reluctant gating mode of glycine receptor channels determines the time course of inhibitory miniature synaptic events in zebrafish hindbrain neurons. *J Neurosci* **18**, 2856-2870 (1998).
4. Harty, T.P. & Manis, P.B. Kinetic analysis of glycine receptor currents in ventral cochlear nucleus. *J Neurophysiol* **79**, 1891-1901 (1998).
5. Balakrishnan, V. & Trussell, L.O. Synaptic inputs to granule cells of the dorsal cochlear nucleus. *J Neurophysiol* **99**, 208-219 (2008).
6. Beato, M., Burzomato, V. & Sivilotti, L.G. The kinetics of inhibition of rat recombinant heteromeric alpha1beta glycine receptors by the low-affinity antagonist SR-95531. *J Physiol* **580**, 171-179 (2007).
7. Alibardi, L. Ultrastructural distribution of glycinergic and GABAergic neurons and axon terminals in the rat dorsal cochlear nucleus, with emphasis on granule cell areas. *J Anat* **203**, 31-56 (2003).
8. Rigo, J.M., Badiu, C.I. & Legendre, P. Heterogeneity of postsynaptic receptor occupancy fluctuations among glycinergic inhibitory synapses in the zebrafish hindbrain. *J Physiol* **553**, 819-832 (2003).
9. Suwa, H., Saint-Amant, L., Triller, A., Drapeau, P. & Legendre, P. High-affinity zinc potentiation of inhibitory postsynaptic glycinergic currents in the zebrafish hindbrain. *J Neurophysiol* **85**, 912-925 (2001).
10. Fucile, S., de Saint Jan, D., David-Watine, B., Korn, H. & Bregestovski, P. Comparison of glycine and GABA actions on the zebrafish homomeric glycine receptor. *J Physiol* **517 (Pt 2)**, 369-383 (1999).
11. Zeilhofer, H.U., *et al.* Glycinergic neurons expressing enhanced green fluorescent protein in bacterial artificial chromosome transgenic mice. *J Comp Neurol* **482**, 123-141 (2005).
12. Barbour, B. & Hausser, M. Intersynaptic diffusion of neurotransmitter. *Trends Neurosci* **20**, 377-384 (1997).
13. Sykova, E. & Nicholson, C. Diffusion in brain extracellular space. *Physiol Rev* **88**, 1277-1340 (2008).